Tectonophysics 833 (2022) 229358

Contents lists available at ScienceDirect

Tectonophysics

journal homepage: www.elsevier.com/locate/tecto

Wide-angle seismic transect reveals the crustal structure of(f) southern Sri Lanka

Tabea Altenbernd-Lang [a,*], Wilfried Jokat [a,b], Wolfram Geissler [a], Christian Haberland [c], Nalin De Silva [d]

[a] Alfred-Wegener-Institut Helmholtz-Zentrum für Polar- und Meeresforschung (AWI), Am Handelshafen 12, 27570 Bremerhaven, Germany
[b] University of Bremen, Department of Geosciences, Klagenfurter Strasse 4, 28359 Bremen, Germany
[c] Geoforschungszentrum Potsdam (GFZ), Albert-Einstein-Strasse 42, 14473 Potsdam, Germany
[d] Geological Survey and Mines Bureau (GSMB), 569 Epitamulla Road, Pitakotte, Sri Lanka

ARTICLE INFO

Keywords:
Indian Ocean
Seismic refraction data
Crustal fabric
Distribution of oceanic crust

ABSTRACT

We present results derived from a seismic refraction experiment and gravity measurements about the crustal structure of southern Sri Lanka and the adjacent Indian Ocean. A P-wave velocity model was derived using forward modelling of the observed travel times along a 509 km long, N-S trending profile at 81°E longitude. Our results show that the continental crust below southern Sri Lanka is up to 38 km thick. A ~ 65 km wide transition zone, which thins seawards to ~7 km thickness, divides stretched continental from oceanic crust. The adjacent, 4.7 to 7 km thick normal oceanic crust is covered by up to 4 km thick sediments. The oceanic crust is characterized by intra-crustal reflections and displays P-wave velocity variations, especially in oceanic layer 2, along our profile. In the central part of the profile, the uppermost mantle layer is characterized by normal P-wave mantle velocities of 8.0–8.1 km/s. At the southern end of the profile, unusual low upper mantle seismic velocities, ranging from 7.5 to 7.6 km/s only, characterize the uppermost mantle layer. These low upper mantle velocities are probably caused by partially serpentinized upper mantle. At even greater depths the upper mantle layer is characterized by velocities of 8.3 km/s on average. The type of margin along our profile is difficult to identify, since it is characterized by features typical for different types of margins.

1. Introduction

Sri Lanka, the island southeast of India in the Indian Ocean, is located at the southernmost part of the Indian subcontinent, which formed a single continent together with Antarctica in the Cretaceous. To reconstruct the initial fit of the continental parts and the early drift history, the knowledge of magnetic spreading anomalies but also the crustal fabric and distribution of continental and oceanic crust is an important constraint.

So far it is known that the evolution of the Indian Ocean took place in several phases (McKenzie and Sclater, 1971; Norton and Sclater, 1979; Powell et al., 1988; Royer and Coffin, 1992). Oceanic crust formation started after the break-up of eastern Gondwanaland during the Early Cretaceous (Curray et al., 1982; Peirce, 1978; Powell et al., 1988). Weak magnetic anomalies in the Bay of Bengal and the resulting uncertainties have led to different theories on the exact location and timing of the onset of early seafloor spreading between 134 and 118 Ma (Banerjee et al., 1995; Desa et al., 2006; Gaina et al., 2007; Jokat et al., 2021; Ramana et al., 1994; Royer and Coffin, 1992). Based on subdued magnetic anomalies, Desa et al. (2006) proposed that the oldest identified magnetic anomaly off the coast of southern Sri Lanka is related to 134 Ma old oceanic crust. In addition, the same authors identified NNW-SSE and NW-SE trending fracture zones south of Sri Lanka, created during this first phase of seafloor spreading. Changes in the orientation of these fracture zones indicate that a major plate reorganization took place in the Late Cretaceous and the Indian plate moved northwards (Johnson et al., 1980; Matthews et al., 2012; Müller et al., 2000). The collision between India and Eurasia at around 50 Ma led to another change in spreading direction to NE-SW until present.

Continental break-up is often accompanied by massive onshore volcanism leading to the formation of flood basalt provinces and intrusions within the stretched continental crust of the conjugate margins.

* Corresponding author.
E-mail addresses: tabea.altenbernd@awi.de (T. Altenbernd-Lang), wilfried.jokat@awi.de (W. Jokat), wolfram.geissler@awi.de (W. Geissler), haber@gfz-potsdam.de (C. Haberland).

https://doi.org/10.1016/j.tecto.2022.229358
Received 14 May 2021; Received in revised form 11 February 2022; Accepted 28 March 2022
Available online 18 April 2022

Not much about onshore volcanism in southern Sri Lanka and its conjugate margin in the Enderby Basin has been reported. Thus, from onshore investigation it seems that the separation of the Antarctica and Indian/Sri Lanka plates happened without major magmatism. The question is if this is also true for the present-day submarine part of the island. The continent-ocean transition zone (COT) is an area which has been affected by stretching of continental crust and subsequent intrusions. Furthermore, this zone can also host an exhumed and serpentinized mantle (e.g. Eagles et al., 2015; Peron-Pinvidic et al., 2013; Whitmarsh and Miles, 1995). The width of the COT, the type of margin and the position of the onset of oceanic crust at the continent-ocean boundary (COB) are important constraints for any kinematic model of

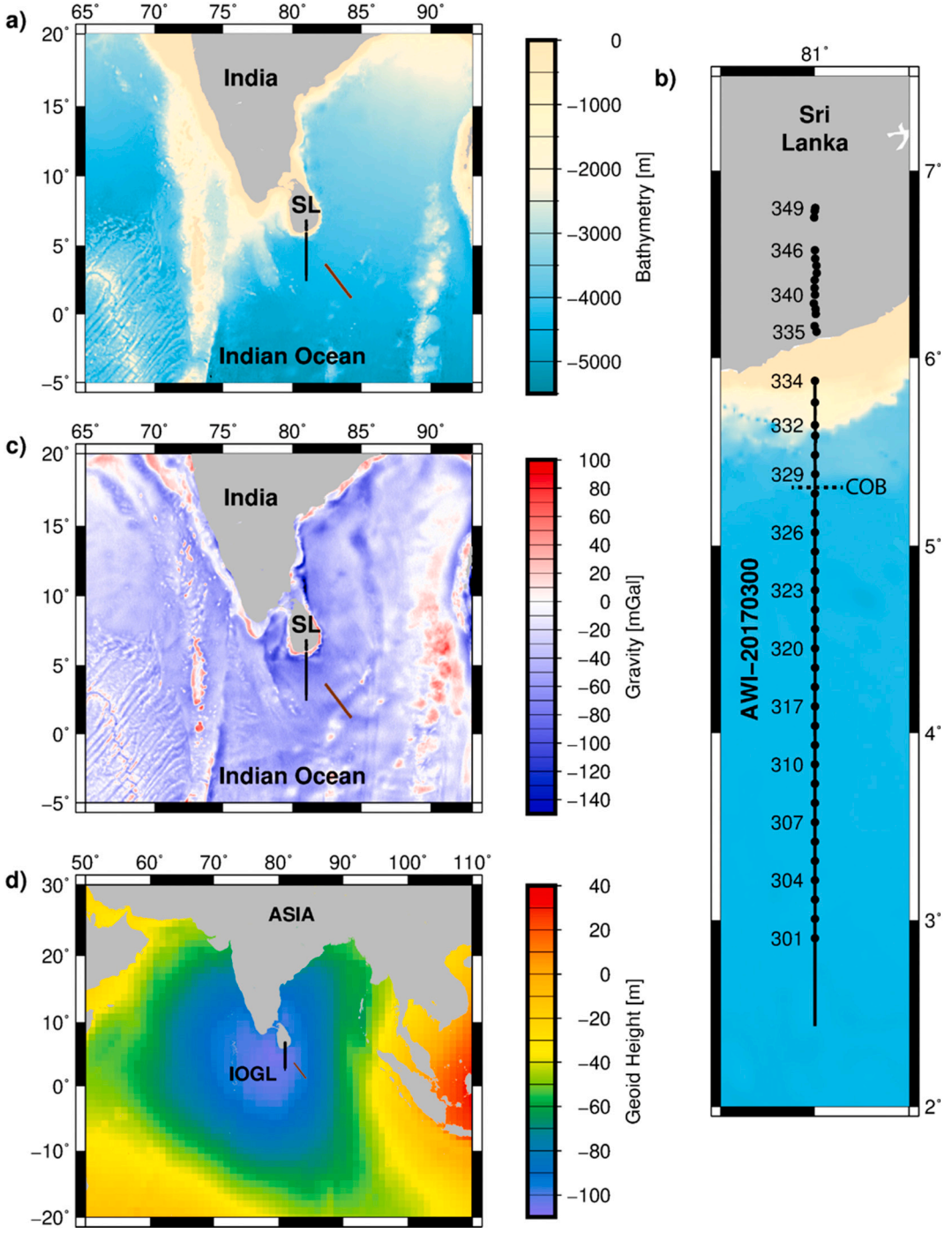

Fig. 1. Bathymetry, gravity and geoid heights in the research area.
a. Bathymetric map (GEBCO_2014 Grid, version 20141103, http://www.gebco.net) with location of profile AWI-20170300 (black line) and AWI-20170400 (brown line, Altenbernd et al. (2020)).
b. Bathymetric map showing the region of interest. The deployment positions of all OBSs and land stations are marked with black circles and annotated with black numbers. The black line marks the location of the shot points. The COB according to Jokat et al. (2021) is marked.
c. Satellite derived gravity map (Sandwell and Smith, 2009).
d. Geoid height (Pavlis et al., 2012). The map shows the location of the IOGL in the Indian Ocean.
Abbreviations: SL: Sri Lanka, IOGL: Indian Ocean Geoid Low

the Indian Ocean. But type, composition and thickness of the crust of southern Sri Lanka and the adjacent oceanic crust have so far mainly been investigated based on few seismological studies (Dreiling et al., 2020; Pathak et al., 2006; Rai et al., 2009), sparse multichannel seismic (MCS) profiles (e.g. Bull and Scrutton, 1990) and potential field data (e.g., Radhakrishna et al., 2010; Rao et al., 2016). Only recently (Jokat et al., 2021), the COB off southern Sri Lanka was better constrained by combining a P-wave velocity model (AWI-20170300) and marine magnetic data along 81°E (Fig. 1). Our contribution uses the same seismic data set. However, here we analyze the seismic wide-angle and

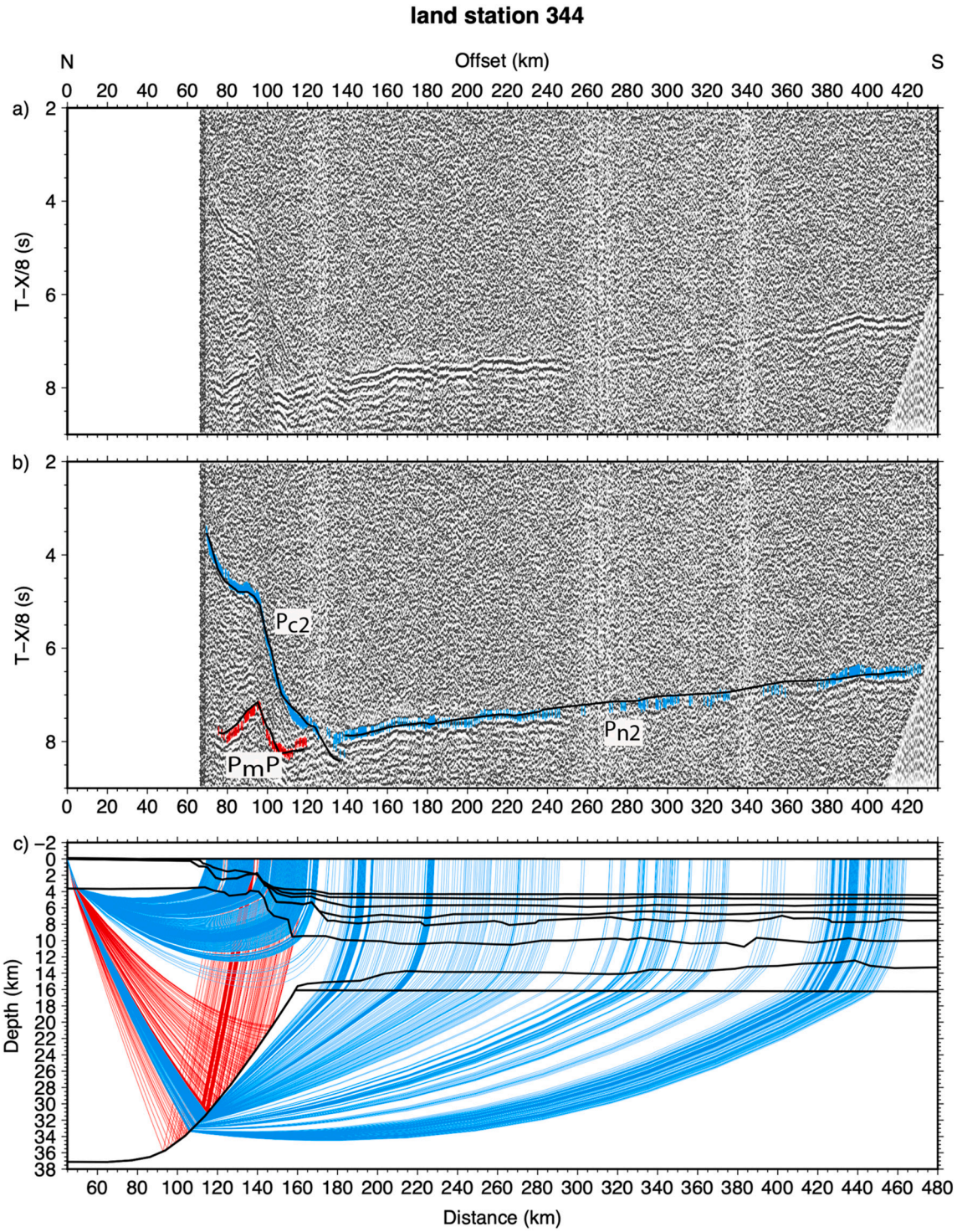

Fig. 2. Seismic record section, picks, and calculated ray paths for land station 344.
a. Seismic record section. The horizontal scale is the shot-receiver distance.
b. Same section as shown above, with picked refractions and reflections shown blue and red, respectively. Phase names are explained in Table 1. The height of the picks depicts the assigned pick uncertainties. The calculated travel times are marked as black line.
c. Calculated raypaths of refracted (red) and reflected (blue) phases within the P-wave velocity model. The horizontal scale is the model distance along the P-wave velocity model.

additionally also gravity data to describe more details of the crustal fabric and uppermost mantle along profile AWI-20170300.

In this context it is important to note that our area of investigation is situated within the Indian Ocean Gravity Low (IOGL), the most prominent geoid low on earth (Fig. 1d). Its evolution and the origin of one or more density anomalies causing the IOGL are still debated. Several theories have been proposed, for example a depression in the core-mantle boundary (Negi et al., 1987), a hot anomaly in the mantle transition zone, underlain by cold anomaly (Reiss et al., 2017), or an uncompensated depression in the upper mantle (Ihnen and Whitcomb, 1983), just to name a few. Our profile provides no information on deeper mantle processes but shed new insights into the structure of the upper mantle in the area of the IOGL.

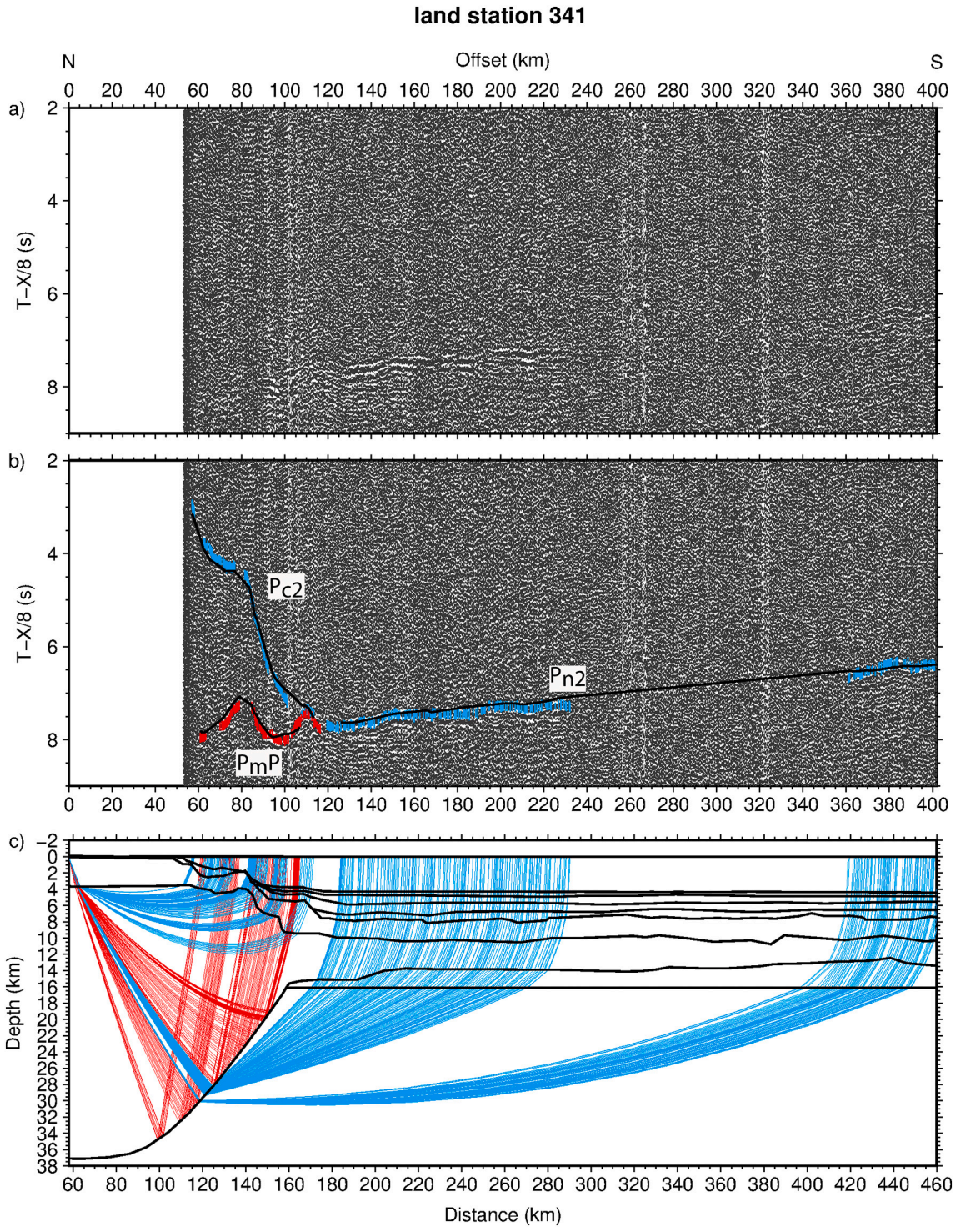

Fig. 3. Seismic record section, picks, and calculated ray paths for land station 341.
a) and b) show the seismic record section, c) the calculated raypaths within the model. For additional explanations, see Fig. 2.

2. Methods

2.1. Acquisition and processing of seismic refraction data

The experiment was carried out onboard RV SONNE in 2017 (Geissler, 2017). Profile AWI-20170300 was acquired along 81°E, using a total of 45 ocean bottom seismometers (OBS) and land stations deployed onshore and offshore (Fig. 1). The instrument spacing of the 30 deployed OBSs on the seafloor was 11.5 km on average. Onshore, 15 land stations were deployed in a distance ranging from 2 to 20 km. Each land station was equipped with a string of 12 geophones. Their GPS clock was synchronized every 15 min.

Different OBS types were used during the experiment. 20 OBSs were equipped with a 3-component broadband seismometer and a hydrophone, while 10 OBSs had a three-component geophone and a hydrophone. A sampling frequency of 250 Hz was used during acquisition. For

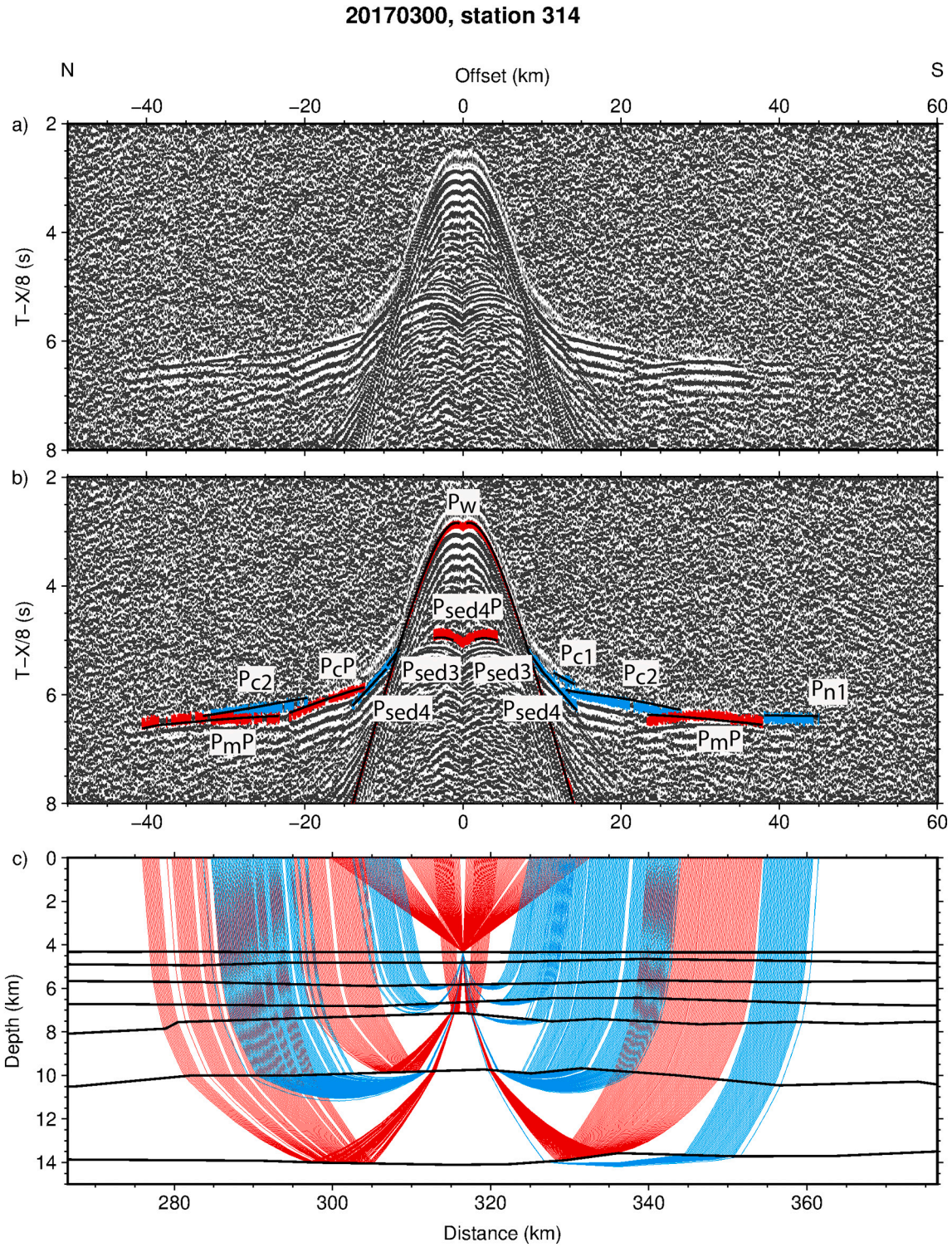

Fig. 4. Seismic record section, picks, and calculated ray paths for OBS station 314.
a) and b) show the seismic record section of the hydrophone channel, c) the calculated raypaths within the model. For additional explanations, see Fig. 2.

more detailed information on instruments and settings, see Geissler (2017).

Shooting was only conducted in the seaward part of the profile and not onshore. An array of 8 G-guns, providing a total volume of 68 l, was operated at 200 bar. The shooting interval was 60 s. Unfortunately, MCS data could not be collected in parallel due to a malfunction of the streamer recording system.

All deployed instruments onshore and offshore along the profile were successfully recovered at the end of the experiment. The recorded raw data were converted to segy format. In addition, the drift of the internal clock was corrected in the OBS data. Also, the OBS locations on the seafloor were corrected for their drift from the deployment position using water-path travel times from the recorded shots. Shot-receiver offsets were calculated and written into the segy headers.

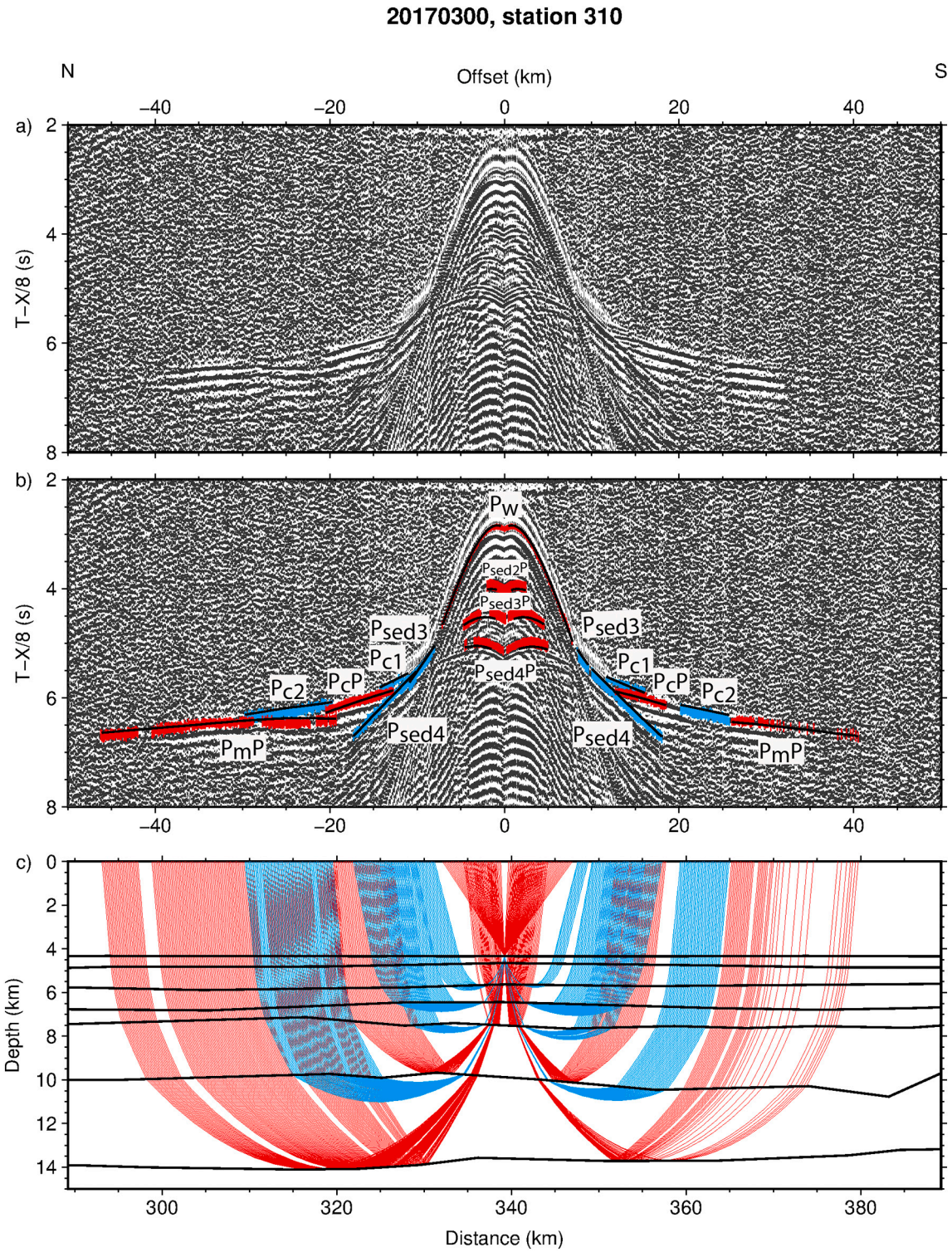

Fig. 5. Seismic record section, picks, and calculated ray paths for OBS station 310.
a) and b) show the seismic record section of the hydrophone channel, c) the calculated raypaths within the model. For additional explanations, see Fig. 2.

2.2. P-wave velocity modelling

We used the open software *zp* for picking first arrivals of refracted and reflected phases (Barry Zelt, http://www.soest.hawaii.edu/users/bzelt/zp/zp.html). The overall data quality was good to excellent. First arrivals could be observed for more than 400 km distance. However, four instruments recorded almost no useable arrivals (stations 307, 318, 322, 336). OBS 328 had a malfunction and recorded no data. Refracted and reflected arrivals within the seismic records were identified based on their amplitude, curvature and velocities. Examples are shown in Figs. 2–8. In the following, refractions through the four sedimentary layers are named P_{sed1}–P_{sed4}, while reflections at the base of the sedimentary layers are named $P_{sed1}P$–$P_{sed4}P$. Refractions in the upper and lower crust are labelled P_{c1} and P_{c2}, respectively. The reflection at the base of the upper crustal layer is named P_cP. Refractions within the mantle below the Moho reflection (P_mP) are named P_{n1} and P_{n2}.

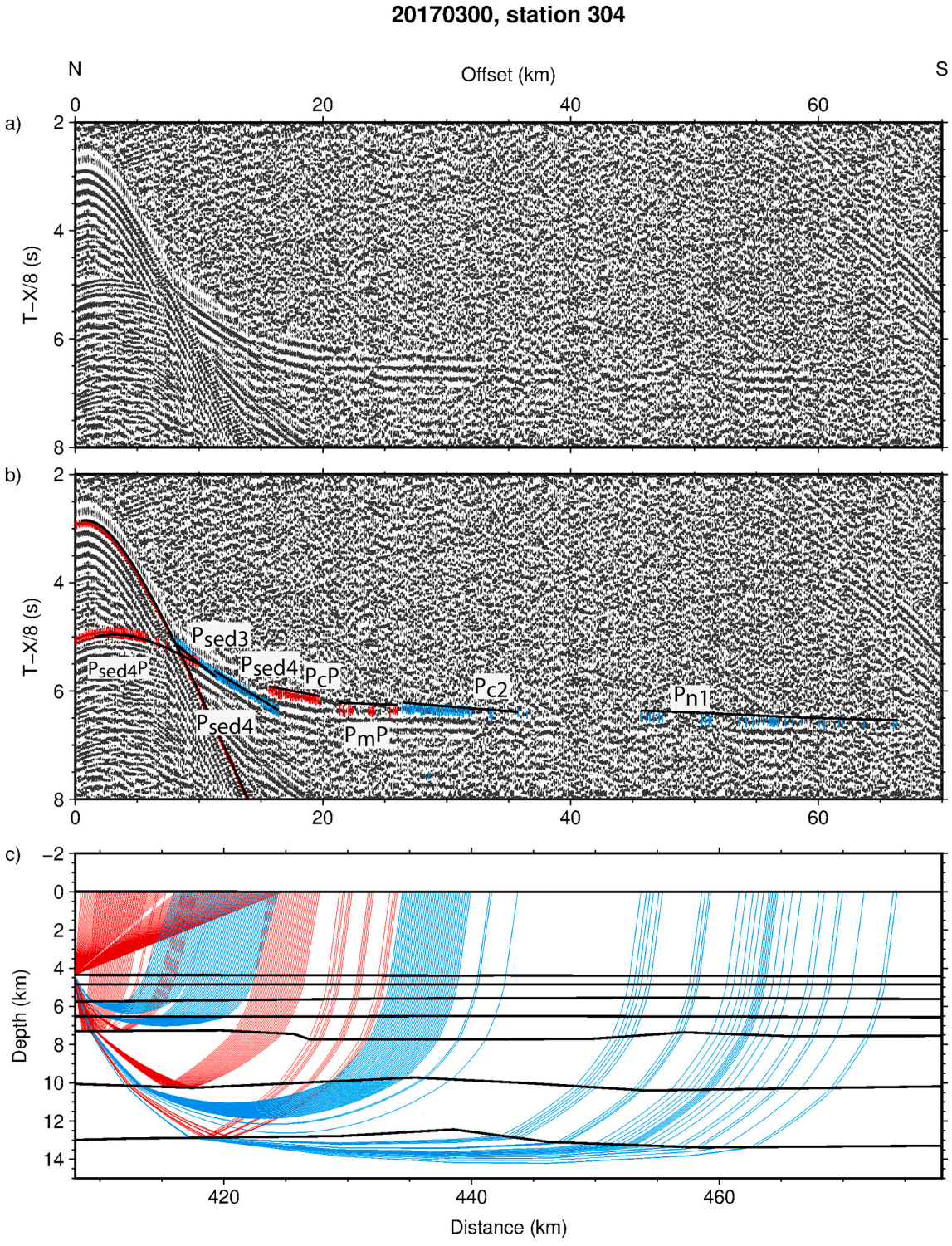

Fig. 6. Seismic record section, picks, and calculated ray paths for OBS station 304.
a) and b) show the seismic record section of the hydrophone channel, c) the calculated raypaths within the model. For additional explanations, see Fig. 2.

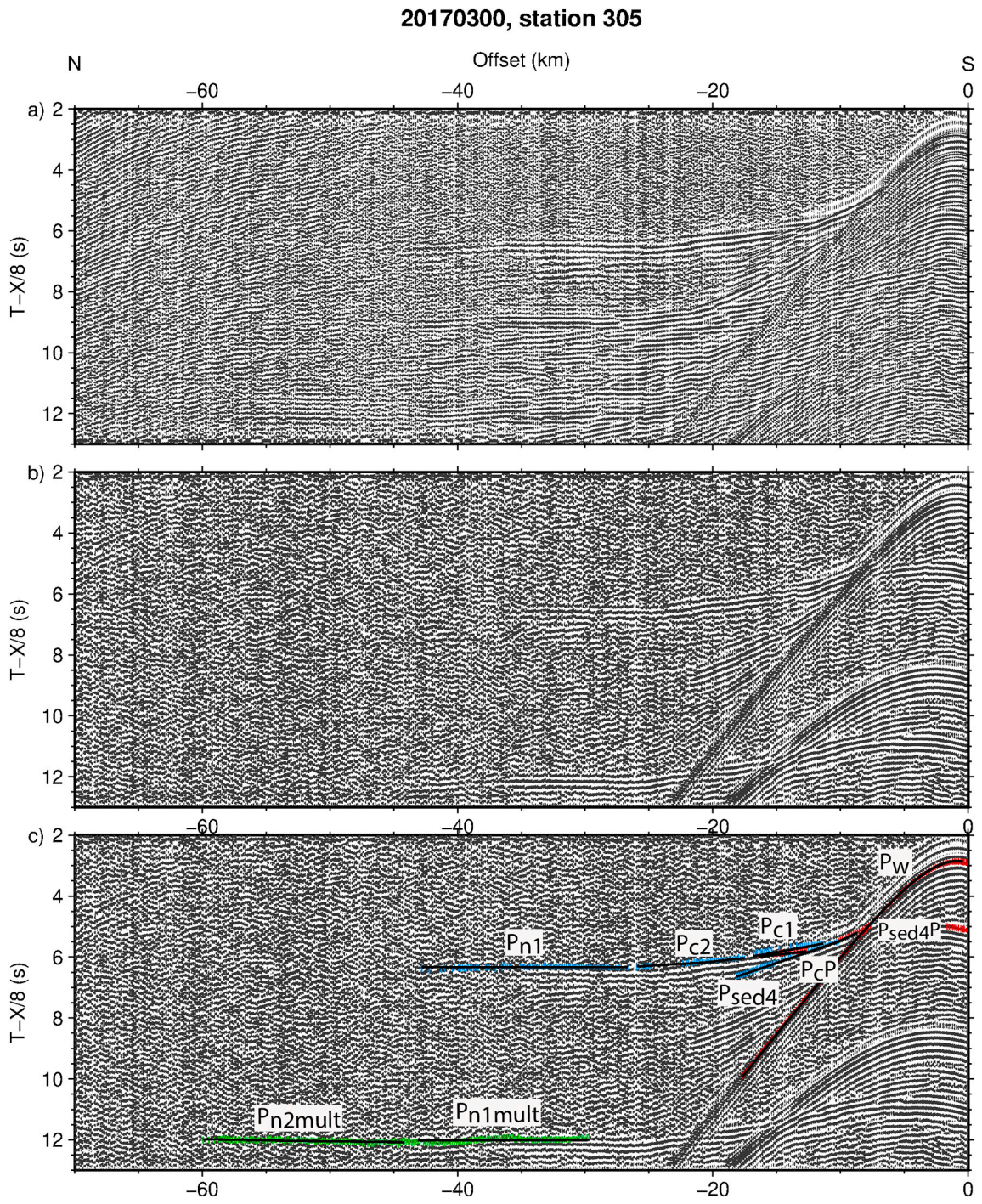

Fig. 7. P_n multiple identified in the seismic record section of OBS station 305.
a. Seismic record section of the z-channel showing strong reverberations masking later arrivals.
b. Seismic record section of the hydrophone channel showing a much better signal quality. The horizontal scale is the shot-receiver distance.
c. Same section as shown in b), with picked multiples of the Pn phases (Pn1mult and Pn2mult). The Pn multiples were picked using data of the z-component of the seismometer (a) and hydrophone channel (b).

Multiples of the P_n refractions are named P_{n1mult} and $P_{n2mult.}$ The naming and number of picked first arrivals are shown in Table 1.

Since we had no MCS data available to obtain information on the sediment and basement geometries along our profile, we applied a special processing to the OBS data to image subsurface structures on either side of our OBS stations (Yelisetti et al., 2017). Removing the move-out of the deep water multiples within the OBS recording with a water velocity of 1.5 km/s, provides in our case a rough image on the subsurface along our profile (for details see Yelisetti et al. (2017)). This information was incorporated into the model setup.

Modelling of the picked first arrivals was conducted with the software rayinvr (Zelt and Smith, 1992) and the graphical interface PRay (Fromm, 2016). Around ~20,000 picks were used for modelling the 509 km long P-wave velocity model by forward and inverse modelling (Fig. 9) from top to bottom. While refractions in the upper sedimentary layers are often masked by the direct wave (P_w), the velocities within the lowermost sedimentary layers, crustal layers, and the upper mantle are very well constrained by numerous refractions in the central and

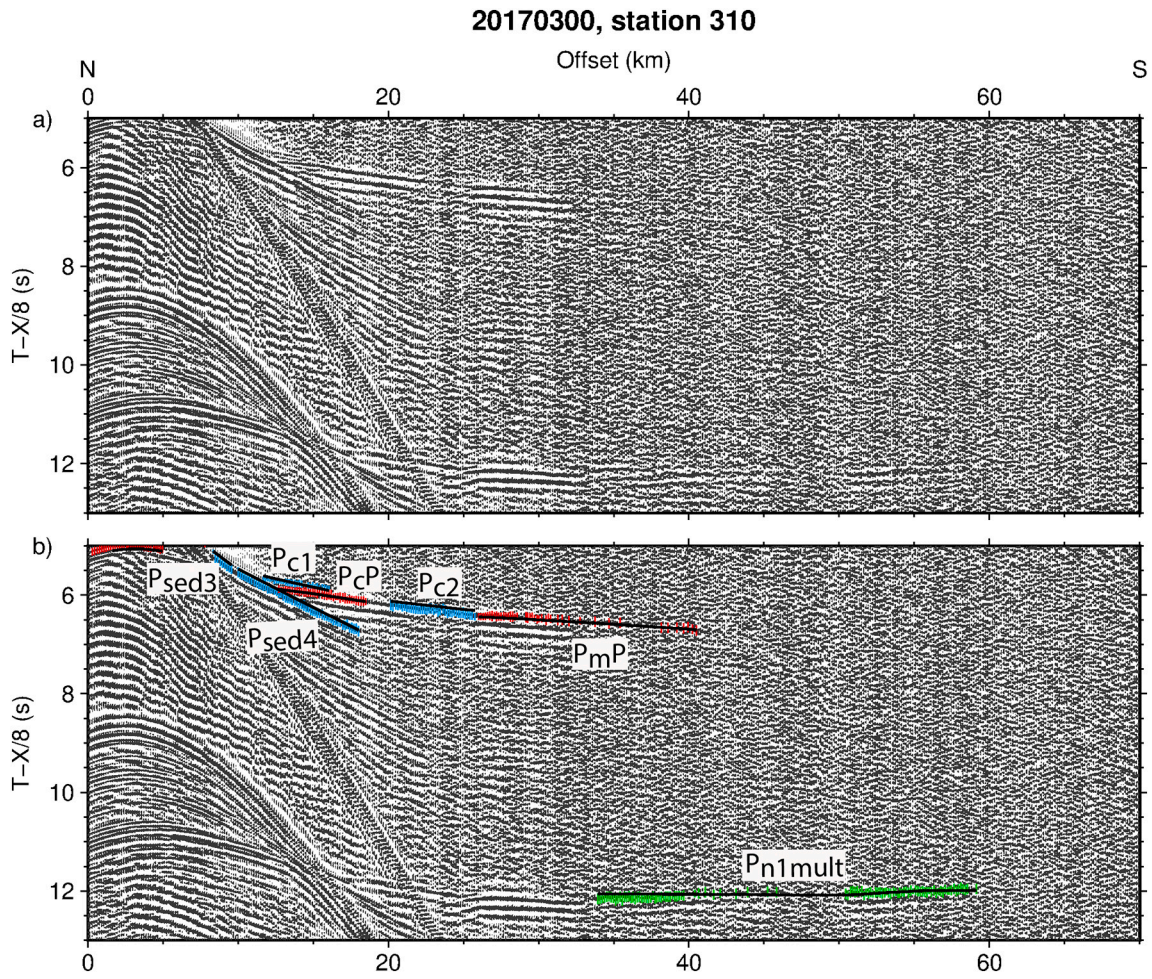

Fig. 8. P_n multiples identified in the seismic record section of OBS station 310.
a Seismic record section of the hydrophone channel. The horizontal scale is the shot-receiver distance.
b Same section as shown above, with picked refractions (blue), reflections (red) and Pn multiples (green). (For interpretation of the references to colour in this figure legend, the reader is referred to the web version of this article.)

Table 1
Description of picked phases, number of picks, RMS misfit between picked and calculated travel times Trms, and chi-squared values.

Phase description	No. of picks	Trms (s)	$\chi 2$
$\mathbf{P_w}$ (direct wave)	4705	0.039	0.285
$\mathbf{P_{sed1}}$ (sediment refractions)	26	0.076	1.108
$\mathbf{P_{sed1}P}$ (sediment reflections)	102	0.047	0.450
$\mathbf{P_{sed2}}$ (sediment refractions)	18	0.054	0.918
$\mathbf{P_{sed2}P}$ (sediment reflections)	20	0.066	0.467
$\mathbf{P_{sed3}}$ (sediment refractions)	738	0.043	0.391
$\mathbf{P_{sed3}P}$ (sediment reflections)	381	0.049	0.265
$\mathbf{P_{sed4}}$ (sediment refractions)	1480	0.043	0.340
$\mathbf{P_{sed4}P}$ (reflection base sediments)	640	0.075	0.699
$\mathbf{P_{c1}}$ (refraction oceanic layer 2 and upper continental crust)	1429	0.074	0.894
$\mathbf{P_cP}$ (reflection base upper crustal layer)	935	0.137	2.896
$\mathbf{P_{c2}}$ (refraction oceanic layer 3 and lower continental crust)	3826	0.086	0.894
$\mathbf{P_mP}$ (Moho reflection)	2724	0.101	1.180
$\mathbf{P_{n1}}$ (refraction in upper mantle I)	624	0.069	0.637
$\mathbf{P_nP}$ (reflection, base serpent. Upper mantle)	24	0.027	0.086
$\mathbf{P_{n1mult}}$ (multiple refraction upper mantle I)	369	0.057	0.413
$\mathbf{P_{n2}}$ (refraction in upper mantle II)	2477	0.077	0.672
$\mathbf{P_{n2mult}}$ (multiple refraction upper mantle II)	131	0.030	0.100
All	**20,649**	**0.075**	**0.756**

southern part of the profile (Fig. 10). Reflections within the crustal layers and some sedimentary layers have been recorded by many stations. The upper crust of the island itself is less well imaged, because of the large initial offsets between the recording station and the first airgun shot at ~114 km model distance (Fig. 9). This results in a very reduced ray coverage for the northern part of the profile. In contrast, the depth of the Moho below the southern part of the island and the COT is very well constrained by a large number of reflections. Especially some of the land stations recorded upper mantle arrivals at very long offsets. Examples are shown in Figs. 2 and 3.

Our P-wave model consists of nine velocity layers (Fig. 9), which were identified based on their P-wave velocities, changes in velocity gradients and reflections at the top and base of layers if present. Up to four layers were needed to model the sedimentary units. Two layers were used to model the continental and oceanic crust along the profile. The crust below Sri Lanka landward of 114 km model distance is poorly constrained due to the experimental setup. Southwards, the velocities of the upper part of the lower crustal layer are constrained by refractions (Fig. 10). We used similar velocities to model the upper crust north of km 114. The velocities of the lower crust in the northern part of the model are constrained by refractions and Moho reflections. These average P-wave velocities of this crustal layer (6.6 km/s) are also in good agreement with tomographic-based results on the crustal structure of Dreiling et al.(2020), who calculated average crustal P-wave velocities of 6.3–6.7 km/s for the Sri Lanka crust. The upper mantle was split into two

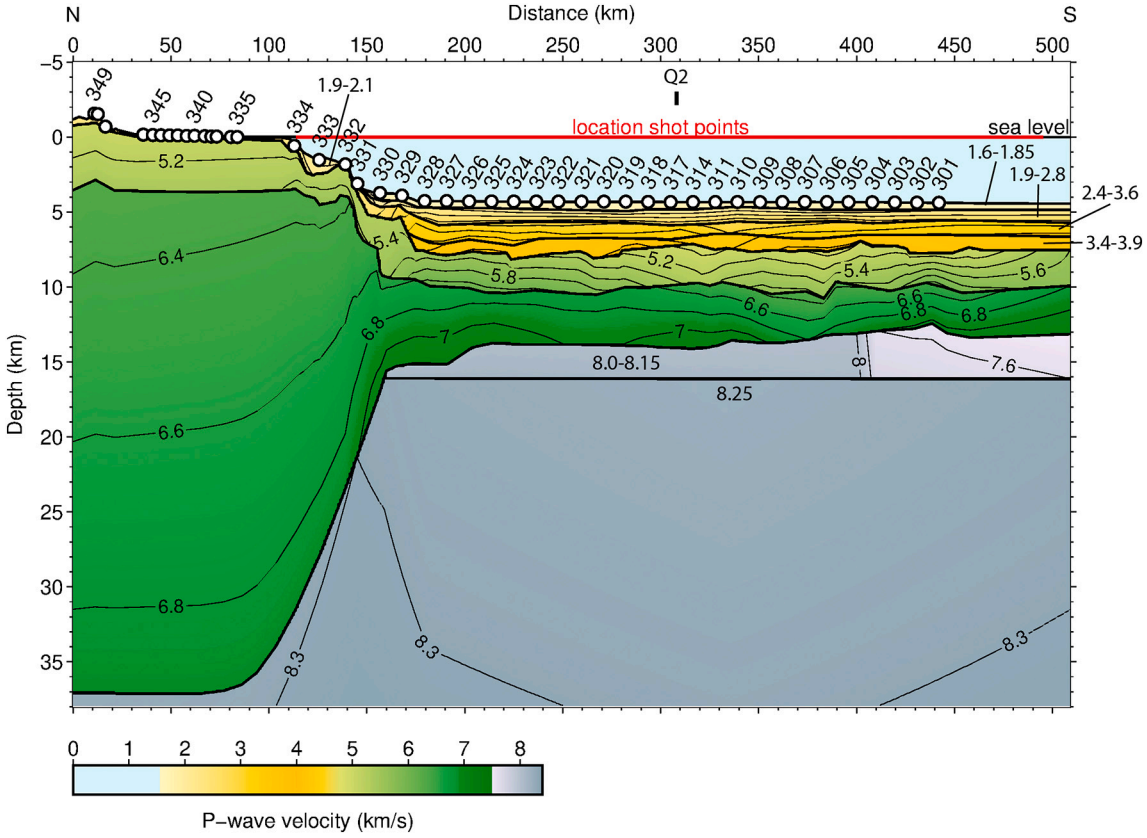

Fig. 9. P-wave velocity model of profile AWI-20170300.
The location of the profile is shown in Fig. 1. Interpreted sedimentary and crustal layers are shown in yellow and green, respectively. The mantle is colored grey. Deployment positions of OBS stations (301−332) and land stations (335–349) are marked with circles and annotated with black numbers. The magnetic field-intensity fluctuation isochron Q2 (108 Ma; Jokat et al., 2021) is marked. The red line marks the locations of the shot points. (For interpretation of the references to colour in this figure legend, the reader is referred to the web version of this article.)

velocity layers in order to account for the observed high mantle velocities on several recording stations.

2.3. Error analysis and uncertainty of the model

Table 1 summarizes the error analysis for individual phases and layers. The normalized chi-squared for the P-wave velocity model is 0.756, which is lower but still close to the optimum value of 1. A normalized chi-squared of 1 means that the fit of the calculated travel times is fully within the assigned pick uncertainties. Therefore, the calculated and observed travel times are in good agreement in our model (Fig. 11). Our estimated pick uncertainties vary between 40 and 100 ms and assigned based on the signal-to-noise ratio. In Figs. 2 to 8, the pick uncertainties are indicated by the height of the bars. The average RMS (root-mean-square) misfit between calculated and picked travel times is 75 ms. The low average RMS misfit shows that the model is well constrained.

Larger errors and uncertainties are to be expected in the northern part of the profile. Because of the experimental setup, only refracted rays covering the upper 16 km of the crust could be detected below Sri Lanka (Fig. 10). Also, no reversed ray coverage is present north of 114 km model distance. The ray coverage in the northern part of the model is reduced since the last shot point is located close to the coast at ~114 km model distance (Fig. 9). As a result, the velocities in this area of our P-wave velocity model are mainly based on crustal refractions in the upper part of the lower crustal layer and the fit of reflections at the Moho. Due to the lack of onshore shots, the crustal structure and P-wave velocities north of 114 km model distance are subject to much greater uncertainties than in the marine area of the profile.

Absolute errors of the model were determined by changing single depth- and velocity nodes of our model and examination of the effects on the calculated travel times. For this we vertically shifted depth nodes or changed the value of velocity nodes until the calculated travel times were outside the range of the pick uncertainty. The following error estimation apply to the range between 40 and 470 km model distance, as no or only sparse ray coverage is present at both ends of the profile. Velocities within sediments, crust and upper mantle are accurate to within ±0.1 km/s south and ± 0.2 km/s north of 170 km model distance. The depth uncertainties for sedimentary and crustal layers increase with depths from 0.1 to 0.4 km south of 170 km model distance. North of 170 km model distance, the depth uncertainties of sedimentary and crustal layers are much greater due to the sparse ray coverage and range between ±0.6 and ± 1.5 km. The uncertainty for the Moho depth is ±1.2 km from 0 to 150 km model distance and ± 0.6 km seawards of 150 km model distance.

2.4. Gravity data acquisition and modelling

Our area of investigation is located within the IOGL (Indian Ocean Geoid Low), the world's most prominent geoid low, situated south of India in the Indian Ocean (Fig. 1d). The relative gravity along our profile was recorded from 113 to 494 km model distance with a Bodenseewerke KSS32-M gravity meter. Tie point measurements were conducted in Colombo before and after the cruise, and the instrumental drift of 5.63 mGal over 86 days was corrected. Also, an Eotvös correction was applied using the ship's GPS positioning records. Measured free-air gravity values along AWI-20170300 range between a maximum of −1 mGal at 113 km model distance to a minimum of −85 mGal at 182 km model

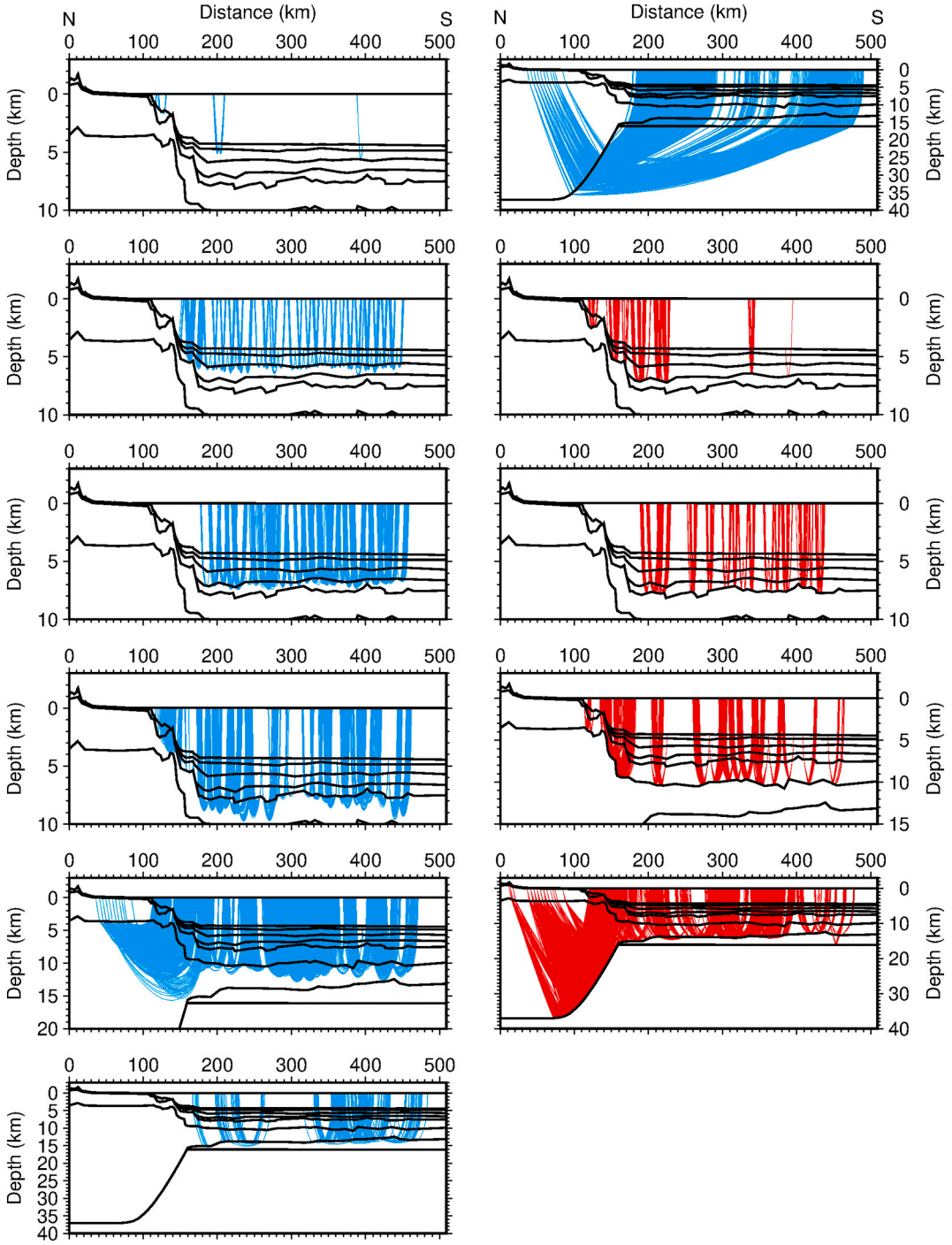

Fig. 10. Ray coverage.
Refracted and reflected rays are shown in blue and red, respectively. The layer boundaries are colored black. (For interpretation of the references to colour in this figure legend, the reader is referred to the web version of this article.)

distance (Fig. 12a).

We performed 2D gravity modelling (Fig. 12) with the software GM-Sys to verify the P-wave velocity model for consistency with the measured free-air gravity data. For our initial density model (start model), average P-wave velocities of the layers were converted to densities based on the generic relationships of Ludwig et al. (1970). The mantle was modelled with a density of 3.3 g/cm^3, except for the upper, presumably serpentinized mantle at the southern end of the model, where a density of 3.25 g/cm^3 was used. If the velocities within a layer changed significantly, the layer was divided into different blocks accordingly. Depth and thickness of the individual layers remained unchanged. The gravity response of our start model in comparison with the measured shipborne gravity anomalies is shown in Fig. 12.

Large misfits between observed and calculated gravity occur south of the shelf in the starting model. Unfortunately, the northern part of our model is partly poorly constrained due to a sparse ray coverage (Fig. 10), which can result in a larger error than in other parts of the model. Therefore, we divided the thick continental crust north of 120 km model distance in two parts and reduced its density from 2.9 g/cm^3 to 2.85 g/cm^3 and 2.88 g/cm^3. By this, a good fit between the measured and

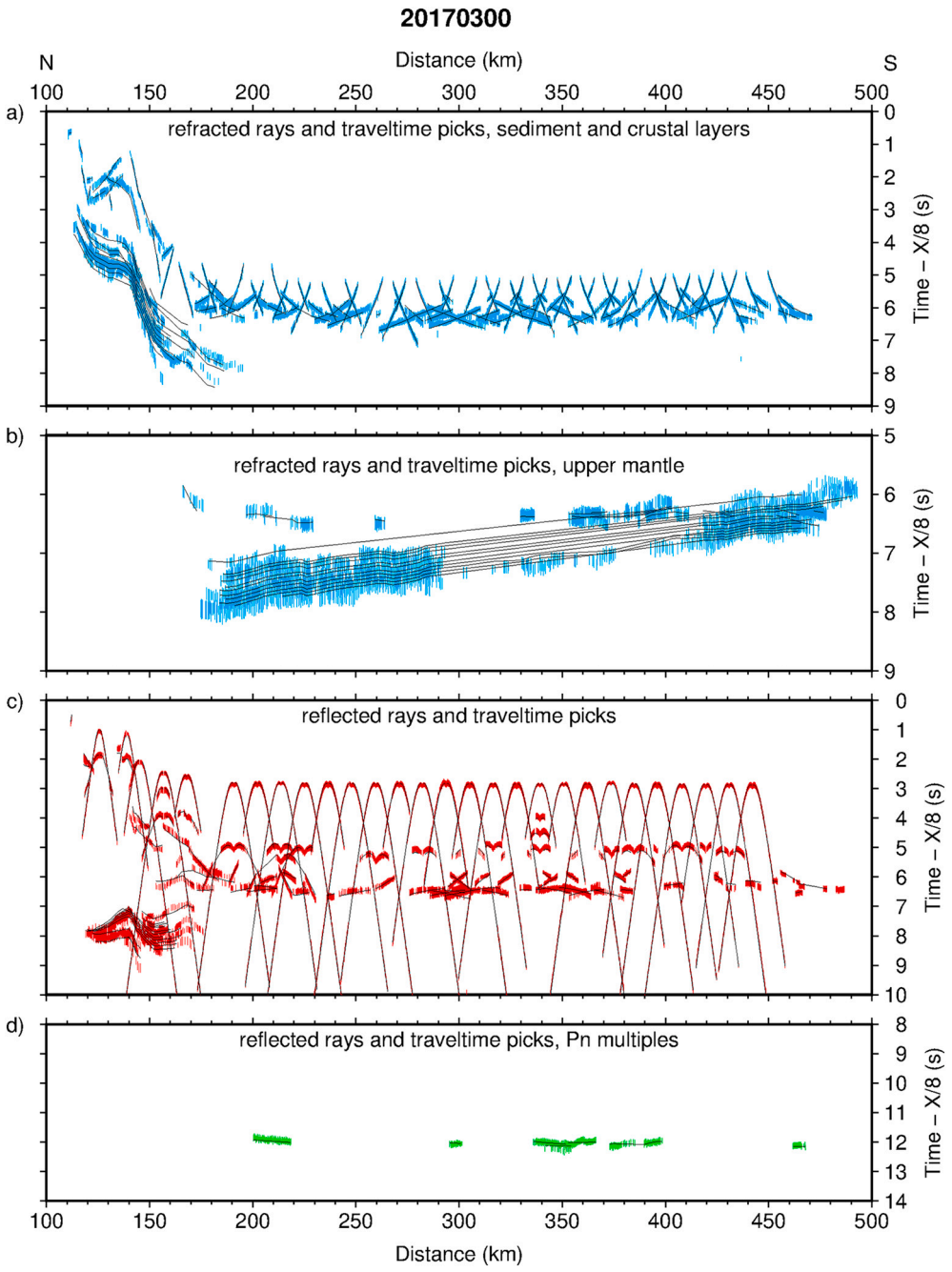

Fig. 11. Fit of picked and calculated travel times.
The height of the picked reflections (red), refractions (blue), and refracted P_n multiples (green) indicates the assigned uncertainties (see also Table 1). (For interpretation of the references to colour in this figure legend, the reader is referred to the web version of this article.)

calculated gravity values is obtained (Fig. 12).

3. Results and interpretation

3.1. Crustal structure and position of the continent ocean boundary and continent ocean transition

The sedimentary cover off southern Sri Lanka is up to 4 km thick in our model (Fig. 9). The velocities of the two uppermost sediment layers are only constrained by very few arrivals and were set to 1.6–1.9 km/s and 1.9–2.8 km/s, respectively. In contrast, the velocities of the lowermost two sedimentary layers are well constrained and range between 2.4 and 3.9 km/s. The crust of Sri Lanka along our profile is up to 38 km thick and thins towards the southern continental margin. The upper crustal layer has a thickness of 2 to 4.5 km, the lower layer has a maximum thickness of 34 km. In this part of the model, velocities lie in the range of 5.0–5.6 km/s in the upper and 6.3–7.0 km/s in the lower part of the crust. Seawards of 175 km model distance, the crust is between 4.7 and 7 km thick. Velocities of the uppermost, 2.2–3 km thick layer range between 4.9 and 5.6 km/s at its top and 5.3 and 6.2 km/s at its base. The underlying, 2.5–5.3 km thick lowermost crustal layer is characterized by velocities of 6.3 to 6.7 km/s at its top and 6.8 to 7.2 km/s at its base. In the lowermost crustal layer, velocities between 330 and 450 km model distance are lower (6.2 to 6.9 km/s) than in the adjacent areas.

To determine the extent and onset of different crustal types

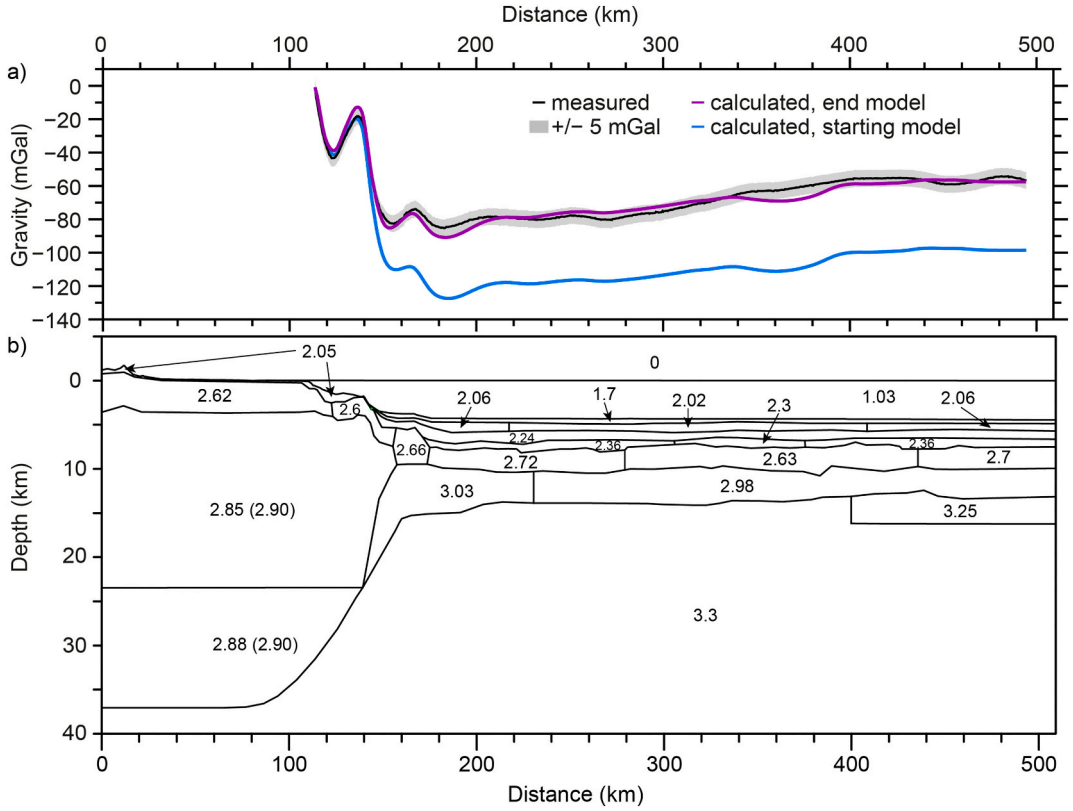

Fig. 12. 2D density model.
a. Measured (black) and calculated free-air anomalies for the start (blue) and end model (purple).
b. Density model derived from the P-wave velocity model. Density values are given in g/cm^3. Values in brackets are densities that were used in the start model and had to be adjusted for the end model.

(continental, oceanic, transitional) along our profile, we calculated velocity-depth functions at various positions (Fig. 13a). Then, we compared these velocity-depth functions with those of normal Atlantic and Pacific oceanic crust (White et al., 1992) (Fig. 13b), with oceanic crust identified in the Indian Ocean along the nearby located profile AWI-20170400 (Altenbernd et al., 2020) (Fig. 13c), and with average and extended continental crust (Christensen and Mooney, 1995) (Fig. 13d,e). Transitional crust within the COT does not have a typical velocity-depth function, in contrast to oceanic and continental crust. The characteristics, P-wave velocities and thicknesses within the COT can vary greatly, as for example serpentinized upper mantle and/or stretched and highly intruded continental crust can be present within the COT.

So far, mainly Atlantic rifted margins, e.g. the Iberian-Newfoundland conjugate margins (e.g. Crosby et al., 2008; Lau et al., 2006) or East Greenland-Norway conjugate margins (e.g. Mjelde et al., 2005; Peron-Pinvidic et al., 2012; Voss and Jokat, 2007), have been investigated in greater detail. As a consequence, characteristics and composition of COTs along rifted margins in many regions of the world are poorly constrained due to a lack of drilling and seismic data. Therefore, we classify transitional crust to be present where the velocity structure or crustal thickness differs significantly from that of typical oceanic or continental crust.

The crust is oceanic between 180 and 500 km model distance. The crustal thickness, velocity gradients and velocity distribution are in good agreement with the crustal structure of Atlantic, Pacific and Indian Ocean oceanic crust. The velocity gradients of oceanic layer 2 (Fig. 13b, blue profiles) are smaller when compared with Atlantic and Pacific oceanic crust, but coincide with those along the closely located profile AWI-20170400 (Fig. 1, Fig. 13c). In comparison with oceanic crust along AWI-20170400, the oceanic crust in our model is in places ~1 km thicker and has lower velocities of 5.0 km/s at the top of oceanic layer 2 in some areas. The oceanic crust shows some velocity variations. Between 300 and 450 km modelling distance, velocities of the oceanic layers 2 and 3 are partly lower than in the adjacent areas, especially in oceanic layer 2 (up to 0.8 km/s) (Fig. 9).

In Fig. 13d and e, we compare the velocity-depth profiles taken between 50 and 170 km model distance with extended and (global-) average continental crust, respectively. From 50 to 100 km model distance, the velocities and velocity gradients lie within the range of average continental crust, and at 125 km and 140 km model distance also for extended continental crust.

While the thickness of the continental crust at 0–80 km model distance remains constant, the crustal thickness decreases seawards, especially south of 110 km model distance. Therefore, we set the onset of the COT at 110 km model distance. Between 150 and 170 km model distance, both the crustal thickness of up to 14 km and the velocity gradient in the upper crustal layer lie outside the typical range of oceanic crust or continental crust (Fig. 13b-e, dark green profiles). However, the velocities in this area in the upper crust are comparable with the adjacent, stretched continental crust, while velocities and velocity gradients in the lower crust are higher. Those higher velocities could be attributed to mafic intrusions at the base of a stretched continental block. Taking these results into account, we place the continent-ocean boundary (COB) marking the onset of oceanic crust in our model at 175 km model distance.

3.2. *Velocities in the upper mantle*

The uppermost mantle layer in our model between 150 and 509 km model distance is 2.5 km thick on average. This P-wave velocity layer was modelled with typical uppermost mantle velocities of 8.0 to 8.15

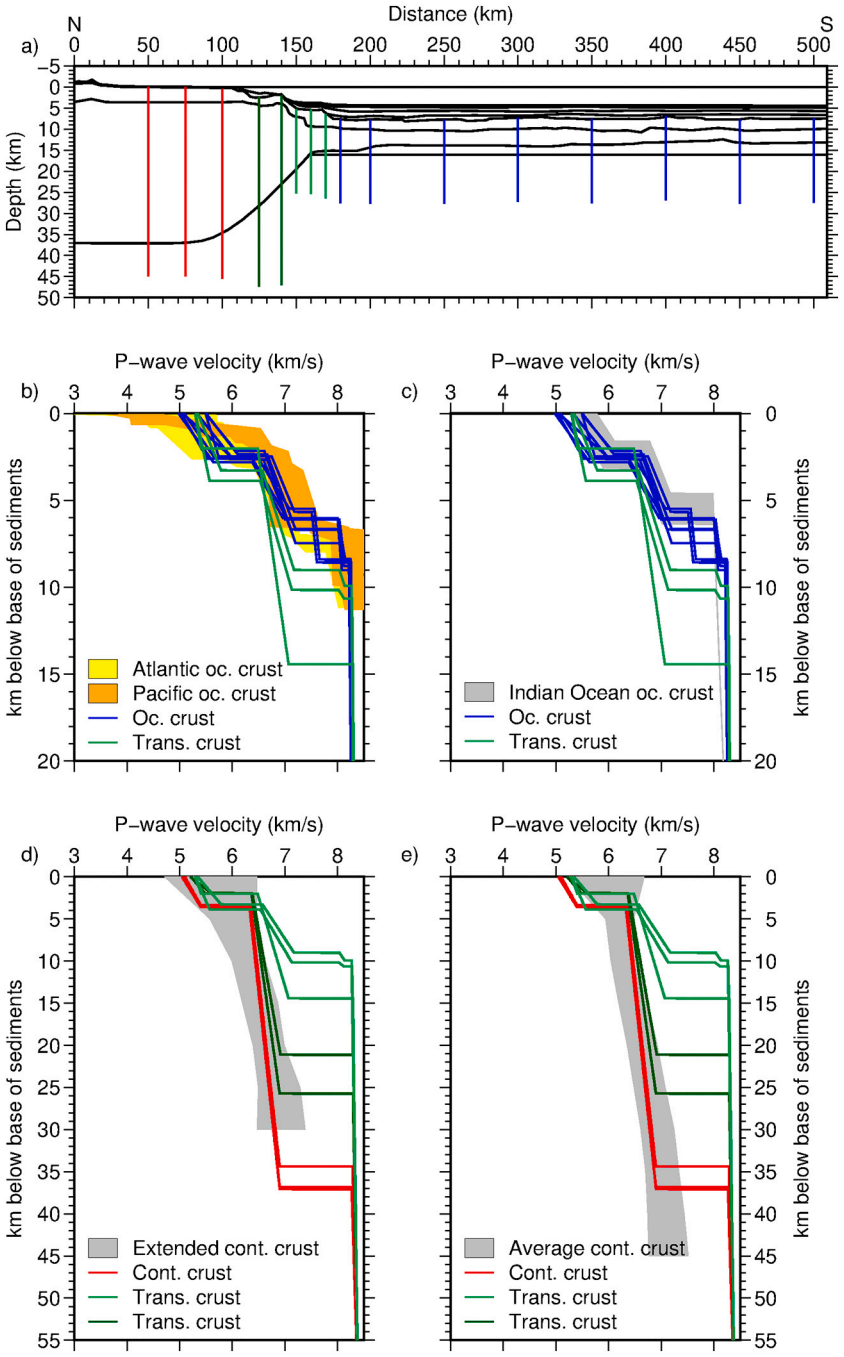

Fig. 13. Comparison of velocity-depth functions taken along profile AWI-20170300 with different crustal types.
a. The location of the different velocity-depth profiles shown in b) to e) are marked with colored lines representing crustal regimes/types: blue: oceanic crust, green: transitional crust, red: continental crust.
b. Comparison of velocity-depth profiles (oceanic and transitional crust) with 59–127 Ma old Atlantic oceanic crust (light grey) and 29–140 Ma old Pacific oceanic crust (dark grey) from White et al. (1992).
c. Velocity-depth profiles of oceanic and transitional crust compared with oceanic crust in the Indian ocean (grey) along AWI-20170400 (Fig. 1a) from Altenbernd et al. (2020).
d. Comparison of continental and transitional crust with extended continental crust (grey) taken from Christensen and Mooney (1995).
e. Comparison of continental and transitional crust with average continental crust (grey) taken from Christensen and Mooney (1995).

km/s and is constrained by refracted arrivals (P_{n1}) identified in several seismic sections (Figs. 4, 10) and some P_{n1} multiples (P_{n1mult}) (Figs. 7, 8). An exception is the area south of 400 km model distance. Here, mantle velocities below the Moho are significantly lower, ranging from 7.5 to 7.8 km/s (Figs. 6, 9). We attribute those low velocities in this part of the mantle to a low degree of serpentinization (<12%) (Christensen, 1966; Horen et al., 1996). In contrast, mantle velocities of up to 8.4 km/s have been recorded by almost all land stations (Figs. 2, 3 and 10). Additionally, multiples of refracted arrivals with normal and higher-than-normal upper mantle velocities were identified in some OBS datasets (Figs. 7, 8). Since the crustal thickness, structure and depth of the Moho is well documented in the oceanic part of the model, we rule out that the observed high mantle P-wave velocities are caused by the Moho dip or topography of the oceanic crust. Hence, a second mantle layer with velocities of 8.25 km/s at its top and 8.45 km/s at its base (70 km depth) was used in our P-wave velocity model to fit the observed upper mantle travel times. The P_n velocities of 8.3 km/s are notably higher than the global average of 8.09 km/s below continents (Christensen and Mooney, 1995). The observed high velocities can be a result of seismic anisotropy, caused by the orientation of olivine crystals in the upper mantle.

4. Discussion

4.1. Crustal structure

Previous studies investigating the Moho depth below Sri Lanka were conducted by receiver function analyses. The determined crustal thickness of southern Sri Lanka ranges between 34 km (Pathak et al., 2006) and 38 km (Rai et al., 2009). Dreiling et al. (2020) studied the crustal

structure of Sri Lanka based on a joint inversion of surface wave dispersion and receiver functions derived from a temporarily installed seismic network consisting of 30 stations. Their results show a Moho depth of 37 to 39 km below southern Sri Lanka. These results agree well with the maximum Moho depth of ~37 km along our profile.

In the past, the presence of oceanic crust and the position of the COB south of Sri Lanka was mainly estimated from potential field data (e.g., Desa et al., 2006). Nevertheless, the new position of the COB (Fig. 1b; Jokat et al., 2021) is close to the gravity-based COB of Desa et al. (2006). Their gravity model predicts the onset of oceanic crust at 145 km model distance (Fig. 14). In our velocity-depth model, it is only located 30 km farther south at ~175 km model distance.

Wide-angle seismic studies investigating the structure of Indian Ocean oceanic crust are sparse (Altenbernd et al., 2020; Kopp et al., 2000; Louden, 1995). Along our profile, the oceanic crust is between 4.7 and 7 km thick. Velocities of the uppermost, 2.2–3 km thick layer range between 4.9 and 6.2 km/s. The underlying lowermost crustal layer was modelled with velocities of 6.3 to 7.2 km/s and has a thickness of 2.5 to 5.3 km. The oceanic crust of the nearby located profile AWI-20170400, acquired with the same acquisition parameters, is between 4 and 7 km thick and partly highly affected by faulting (Altenbernd et al., 2020). As shown in Fig. 13c, the characteristics of the oceanic crust along both profiles (AWI-20170400 and AWI-20170300) are very similar. However, the minimum thickness of oceanic crust in both mentioned profiles is below the (global-) average crustal thickness of 7.1 km (White et al., 1992) or 6.2 km (Christeson et al., 2019) for oceanic crust. The partly lower-than-normal thickness of the oceanic crust is also in good agreement with the characteristics of the oceanic crust in the Central Indian Ocean, where seismic refraction measurements imaged an area of highly deformed crust (Louden, 1995). A total crustal thickness of only 5.4–6.2 km was calculated, with P-wave velocities of 4.5–6.8 km/s in the upper oceanic crustal layer and 6.4–7.4 km/s in the lower oceanic crustal layer (Louden, 1995). In contrast to our profile, the crust is highly deformed and the lower crustal layer is partly characterized by low velocity zones (6.5–7.8 km/s) beneath basement ridge crests.

As already mentioned, the intra-crustal reflections at the boundary between oceanic layer 2 and oceanic layer 3 are not a typical characteristic of oceanic crust. However, there are other examples of these unusual reflections occurring within the crust from the Indian Ocean. In the Mozambique Basin, the oceanic crust is 5.5–7 km thick, with velocities of 5.6–5.8 km/s in layer 2 and 6.5–7.0 km/s in layer 3 (Mueller et al., 2016), and intracrustal reflections occur almost everywhere at the base of oceanic layer 2. The existence of oceanic crust in the Mozambique Basin is well constrained by magnetic spreading anomalies (e.g. Simpson et al., 1979; Leinweber and Jokat, 2012; Mueller and Jokat, 2019). It is therefore unlikely that the crustal structure in the P-wave velocity model was misinterpreted. In contrast to the Mozambique Basin, no clear magnetic spreading anomalies have been identified south of Sri Lanka in our research area. Based on magnetic data collected in 2017, Jokat et al. (2021) identified field-intensity fluctuations Q2 (108 Ma) at 310 km model distance (Fig. 9) and Q1 (92 Ma) south of our profile. Only some hundred km southeast of our profile, intra-crustal reflections have also been identified in the oceanic crust underlying AWI-20170400 (Altenbernd et al., 2020) (Fig. 1).

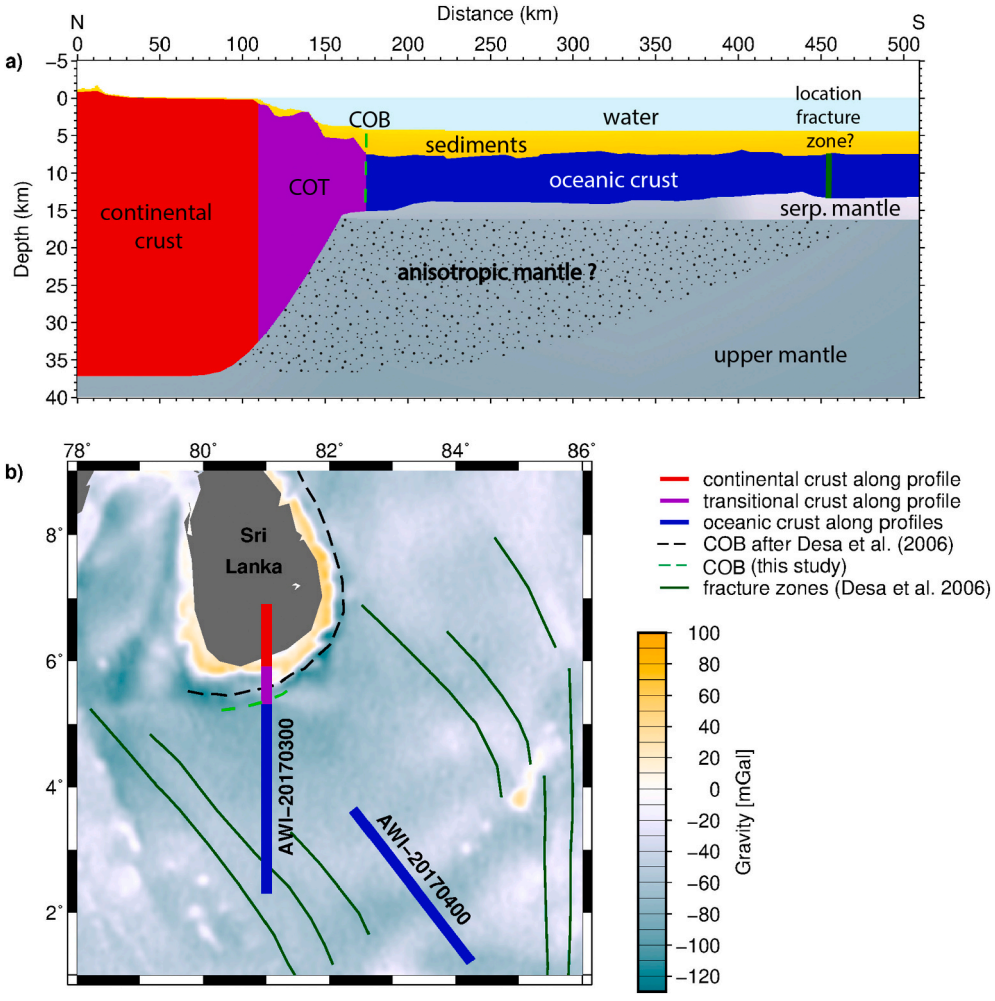

Fig. 14. Interpretation of the seismic results.
a) Crustal types along profile AWI-20170300 shown in Fig. 9.
b) Distribution of different crustal types along AWI-20170300 and the position of the COB after Desa et al. (2006) and this study. Abbreviations: COB: continent-ocean boundary; COT: continent-ocean transition; serp. mantle: serpentinized upper mantle.

Normal oceanic crust specifically in the deep abyssal plains is rarely investigated, as seismic refraction measurements are mainly carried out across continental margins, LIPs or mid-ocean ridges. The quality of the data has also increased significantly in recent decades due to improved technology. Therefore, in our opinion, it is entirely possible that intra-crustal reflections at the layer 2/3 boundary occur much more frequently than previously thought, or that the oceanic crust in the Indian Ocean differs in this respect from the Atlantic and Pacific crust structure. Finally, since the velocity-depth profile of the oceanic crust along AWI-20170400 shows many similarities with the crust south of 175 km model distance along our profile, we are confident that this crust is, despite its intra-crustal reflections, oceanic.

4.2. Variations in the oceanic crustal velocities

The oceanic crust, especially oceanic layer 2, is characterized by velocity variations (Fig. 9). Between 250 and 350 km model distance, velocities of oceanic layer 2 are lower than to the south and north. Variations of oceanic crustal velocities have been reported from other regions. Along the Western Barent Sea margin, Libak et al. (2012) identified strong velocity variations in oceanic layer 2, while velocities in oceanic layer 3 remain relatively constant. Variations in the crustal velocities of oceanic crust may be caused by variations in lithology, age or alteration. For example, crustal accretion and the structure and thickness of oceanic crust often depends on the spreading rate and magma supply (Christeson et al., 2019; Dick et al., 2003; White et al., 1992). Klingelhoefer et al. (2009) identified oceanic crust with high lower crustal velocities ("high velocity oceanic crust") west of the southern Moroccan continental margin. After Klingelhoefer et al. (2009), a possible explanation might be that the oceanic crust contains high amount of serpentinite formed as a result of slow spreading rates.

Suckro et al. (2012) report a high variability of oceanic layer 2 velocities in the oceanic crust of southern Baffin Bay. Based on these velocities, Suckro et al. (2012) divided the upper crust into basalts (4.2–5.7 km/s) and underlying dykes (5.5–6.4 km/s). The thickness of the basalts and dykes varies significantly, which also results in a high variability of the P-wave velocities. Funck et al. (2012) divided oceanic layer 2 in the southern Baffin Bay into segments with different velocities (5.5–6.0 km/s and 6.1–6.5 km/s) and thicknesses. These segments are probably separated by fracture zones and were formed at different ages (Funck et al., 2012). Our profile was acquired in a 45° angle to the spreading direction (Figs. 1, 14). It is therefore likely that our profile crosses more than the one fracture zone shown in Fig. 14 and that the variations in crustal velocities can be explained by segmented lithosphere formed at different ages and different conditions. Differences in the degree of alteration can also be responsible for the velocity variations. However, a more detailed interpretation of the observed velocity variations cannot be provided by a single regional profile.

4.3. Type of margin

The experimental setup, the lack of onshore shots, and missing MCS data make it difficult to determine the type of margin (magma-poor, magma-rich, transform) along our profile. Additionally, our profile is also not oriented perpendicular to the spreading direction and crosses the fracture zones south of Sri Lanka at an angle of ~45° (Fig. 14b), which makes identification of the type of margin even more difficult.

The COT in our model is characterized by rifted and extended continental crust and is in general considerably thinner (7–30 km) than the adjacent, ~38 km thick continental crust. The resulting stretching factor of max. ~5 is typical for a magma-poor rifted margin (Mjelde et al., 2007). Rotated fault blocks might be present between 110 and 175 km model distance (Fig. 9), which is another characteristic for this type of margin. However, clear indications for serpentinized upper mantle, often observed within the COT on magma-poor margins (Chian et al., 1999; Mjelde et al., 2007), are missing in the COT of our model. Wide zones of exhumed upper mantle, which separate the extremely thinned continental crust from oceanic crust, (e.g. Dean et al., 2000; Reston, 2009; Whitmarsh et al., 2001), are also missing along our profile. Since the upper mantle in the COT of magma-poor margins is often completely serpentinized, the P-wave velocities increase gradually from the basement to the upper mantle. Moho reflections are weak or missing (Dean et al., 2000), therefore, no abrupt increase of the P-wave velocity at the Moho is likely.

Indications for a magma-rich margin are signs for massive volcanic activity during its formation. A typical structural element for magma-rich rifted margins are Seaward Dipping Reflectors (e.g., Eldholm et al., 1987; Gladczenko et al., 1998; Hinz, 1981). Due to the lack of MCS data along our profile, we cannot say whether Seaward Dipping Reflectors (SDRs) or massive intrusions are present along the margin. Another characteristic of a magma-rich margin are high-velocity lower crustal bodies (P-wave velocities of 7.2–7.7 km/s) underneath the transitional crust (Geoffroy, 2005; Holbrook et al., 2001; Kelemen and Holbrook, 1995; White et al., 1987). High seismic velocities of up to 7.2 km/s (±1 km/s) are present between 140 and 250 km model distance. But these high velocities in the lower crust are close to the lower limit of P-wave velocities typical for high-velocity crustal bodies. Looking at the determined uncertainties of ~0.1 km/s, the velocities can also be too low to indicate underplating. Massive intrusions within the stretched continental crust of the transition zone, identified along other magma-rich margins (e.g. Abdelmalak et al., 2015; Mutter et al., 1984), are also not visible in our data.

The third possible margin type is the transform margin, which normally displays a sharp continent to ocean transition (e.g. Sage et al., 2000). Such a sharp transition can be discerned by adjacent crustal sections characterized by different velocities and thicknesses. In contrast to that, we identified a transition zone along our profile between 110 and 175 m model distance (Fig. 9). While some transform margins are characterized by steep Moho slopes (higher than 10°), others are characterized by a gentle slope (Mercier de Lépinay et al., 2016). The continental Moho slope between 110 and 150 km model distance is highly variable and partly very steep (up to 20°). Compared to divergent margins, transform margins have a narrow necking zone (50–100 km) in the zone of stretched continental crust (Mercier de Lépinay et al., 2016). The necking zone in our model is within the range typical for transform margins. A marginal ridge at the edge of the continental slope is sometimes present at transform margin (Berndt et al., 2001; Døssing et al., 2010; Mercier de Lépinay et al., 2016). The two basement steps between 120 and 140 km model distance, and 150 and 170 km model distance (Fig. 9) could be interpreted as such, but could also display structures related to extension, like fault blocks.

In summary, it is not possible to unequivocally assign the continental margin of our profile to one type of continental margin, since some, but never all, of the characteristics are met. This is not surprising given the orientation of the profile and history of Sri Lanka's separation from the conjugate continental margin in Antarctica. The conjugate margin of southern Sri Lanka is located in the Lützow-Holm Bay area (Gaina et al., 2007; Jokat et al., 2021). In the first phase of the separation, slow oblique continental extension in the Lützow-Holm Bay area took place (Jokat et al., 2021). After a phase of counterclockwise rotation of Sri Lanka, the first oceanic crust adjacent to southern Sri Lanka was formed around 112 Ma (Jokat et al., 2021). The evolution of the margin is therefore complicated, and the margin type can best be described as an oblique rifted, divergent margin which was affected by strike-slip motion in its early formation.

4.4. Serpentinized upper mantle

We attribute low velocities in the upper mantle south of 400 km model distance at a depth of 8–12 km below the seafloor to serpentinization (Fig. 9). South of 470 km model distance, the ray coverage of the "serpentinized" mantle is sparse or absent (Fig. 10, lower left and top

right). Therefore, the southern extent of the serpentinized section might be smaller than indicated in our model. However, the gravity model (Fig. 12) indicates that also the area south of 470 km model distance is underlain by material with lower densities.

Delescluse and Chamot-Rooke (2008) interpret bright reflectors in MCS data at a Moho depth level (8–15 km below the seafloor) as serpentinization fronts in the Central Indian Basin. Deep faults cut through the entire oceanic crust and offset the Moho leading to sea water infiltration into the uppermost mantle and an exothermic serpentinization reaction. Due to the lack of seismic reflection data parallel to our wide-angle profile, we do not have any direct evidence that the crust and Moho are highly faulted. The thickness of the crust overlaying the serpentinized upper mantle derived from the seismic refraction data is in parts significantly thinner (~5 km at 435 km model distance, Fig. 9) than in other areas of the profile. A further indicator for faulting in that area is the position of a fracture zone, which crosses our profile at its southern end (Fig. 14), in an area probably underlain by serpentinized upper mantle. The fracture zone can explain how pathways for sea water evolved, leading to serpentinization of the very upper mantle material in its vicinity.

4.5. Possible reasons for high velocities in the upper mantle

The high velocities in the upper mantle are the most surprising result of our experiment and can be a result of seismic anisotropy. P-wave anisotropy in the upper mantle is known from refraction experiments both on continents and in the oceans. It is often a result of shearing due to mantle flow. Shear caused by convective mantle flow can result in lattice-preferred orientation (LPO) of olivine crystals (e.g., Hess, 1964; Jung and Karato, 2001; McKenzie, 1979; Tanimoto and Anderson, 1984), leading to seismic anisotropy beneath continents (e.g., Heintz et al., 2009; Pavlenkova, 1996) and oceans (e.g., Gaherty et al., 2004; Hess, 1964; Shearer and Orcutt, 1985).

High mantle velocities are often observed in areas affected by mantle plumes or hotspot tracks (e.g. Grevemeyer et al., 2001; Stern et al., 2020). A high velocity layer within the upper mantle has been found below the Ninetyeast Ridge in the Indian Ocean (Grevemeyer et al., 2001). Here, velocities of 8.4 to 8.6 km/s characterize an anisotropic layer below an upper mantle with normal mantle velocities. Grevemeyer et al. (2001) explain this anisotropic layer with alignment of olivine crystals due to the flow of the plume material which formed the ridge. High P-wave velocities of 8.6 to 9.0 km/s in the upper mantle below the Ontong-Java-Manihiki-Hikurangi Plateau have been explained by LPO orientation related to gravitational spreading (Stern et al., 2020). These authors state that late-stage collapse and spreading of large mantle plumes leads to a radial anisotropy. High water content and stress can also lead to a fast direction orthogonal to the direction of mantle flow (Jung and Karato, 2001). Mantle velocities of ~8.3 km/s have been identified along a line crossing the Louisville Hotspot chain and oriented approximately orthogonal to the spreading center (Contreras-Reyes et al., 2010). In contrast to most of these studies our research area is far away from any known hotspot- or plume track and no indications that the crust was affected by massive volcanism or magmatism have been identified. Thus, it is highly unlikely that a possible anisotropy in the upper mantle is caused by a plume- or hotspot track.

LPO under oceanic crust can also be linked to seafloor spreading. The P_n velocity is highly depending on the azimuth (Hess, 1964), and the maximum P_n velocity correlates with the direction of seafloor spreading (Raitt et al., 1971). Examples of P_n anisotropy related to seafloor spreading and mantle flow direction are known from the Atlantic and Pacific Ocean (e.g. Gaherty et al., 2004; Shearer and Orcutt, 1985; Shinohara et al., 2008). It is known that spreading rates can have an effect on the magnitude of lithospheric P-wave anisotropy, with anisotropy created by slow spreading having a smaller magnitude than in areas with fast spreading rates. Gaherty et al. (2004) reported a P-wave anisotropy of 3.4% along a seismic refraction profile in the western Atlantic and investigated why the magnitude is smaller than in the Pacific. According to them, the LPO of olivines is less organized in regions with slow seafloor spreading, resulting in a smaller anisotropy. Oikawa et al. (2010) reported mantle velocities of up to 8.7 km/s below an up to 3 km thick layer with normal P_n velocities of 8.0 km/s in the Pacific. Since their profile is aligned parallel to the spreading direction in the Northwest Pacific Basin, the high P_n velocities indicate a velocity anisotropy of 7–10% of the upper mantle. Our profile is aligned at an angle of ~45° to the paleo-spreading direction of the Cretaceous oceanic crust, as documented by fracture zones (Fig. 14b). If the anisotropy is a result of seafloor spreading, P_n velocities along the close by profile AWI-20170400, which is nearly aligned parallel to the spreading direction, should be much higher in the upper mantle than along our profile, which is not the case. However, it has to be kept in mind that P_n first arrivals associated with high velocities of up to 8.4 km/s were mostly recorded by the land stations along our profile. These P_n arrivals cover and resolve a deeper and wider area than the P_{n2mult} arrivals imaged by the OBSs. The AWI-20170400 data set in the southeast (Figs. 1, 14b) indicates that the upper mantle is underlain by mantle with normal velocities of 8.0 km/s. But an anisotropic area is probably located deeper than the area imaged by the OBSs along the profile. A spreading-related origin of the high mantle velocities can therefore not be ruled out.

When discussing the origin of the high mantle velocities and a possible mantle anisotropy one has to keep in mind that our research area is situated within the Indian Ocean Geoid Low (IOGL) (Fig. 1d). Different theories for its formation have been discussed in the last decades, such as a depression of the core-mantle boundary (Negi et al., 1987), a subducted slab of the Indian plate (Mishra, 2014), or an isostatically uncompensated depression (Ihnen and Whitcomb, 1983). After Reiss et al. (2017) and Rao et al. (2020) it is the result of a combination of hot material in the mid mantle underlain by cold material of an old slab. After Ghosh et al. (2017), the geoid low is the result of an elongated, low-density anomaly at 300–900 km depth caused by hot material of a low-density plume, migrating from the African large low shear velocity province (LLSVP) to the Northeast.

Our data base is not sufficient to add new knowledge to the above theories. However, the high upper mantle velocities close to the island might indicate that the processes causing the IOGL could also affect shallow upper mantle structures. Currently, not enough is known about flow directions causing LPO in the shallow upper mantle. The origin or composition of the density anomalies causing the IOGL are not well constrained to judge if the high P_n velocities along our profile are related to the IOGL. It is therefore quite conceivable that our observation is related to processes causing the IOGL.

5. Conclusion

We present the first seismic refraction profile constraining the transition from continental to oceanic crust south of Sri Lanka. Our findings show that the crust along profile AWI-20170300 can be divided into continental, transitional and oceanic crust with average thicknesses of 38, 20 and 6 km, respectively. The thickness of the oceanic crust is ~1 km less than that of (global) average oceanic crust. Intra-crustal reflections at the oceanic layer 2/3 boundary are present along our profile. Since this observation has already been made along another nearby profile, it is possible that the Indian Ocean oceanic crust differs in this respect from oceanic crust of other areas. Velocity variations in the oceanic crust along our profile, which can be observed especially in the upper oceanic crustal layer, can be a result of crustal segments of different ages, separated by fracture zones.

The COT has a width of ~65 km along our profile and is characterized by stretched continental crust. The type of margin is difficult to identify due to the orientation of the profile and missing MCS data. The margin along our profile shows characteristics typical for different margin types and can best be described as oblique rifted, divergent margin which was also affected by strike-slip motion during its

formation.

Serpentinized upper mantle with low velocities of 7.5 to 7.8 km/s is present in an area affected by a fracture zone at the southern end of our model. North of the fracture zone, the upper mantle velocities directly below the Moho are normal (8.0 km/s). Just 2.5 km below the base of the oceanic crust, the upper mantle is characterized by high P-wave velocities of ~8.3 km/s. The oceanic crust is underlain by upper mantle characterized by velocities of 8.0–8.1 km/s in the upper kilometers. One explanation for the unusual high mantle velocities could be seismically anisotropic upper mantle. The relevant process causing the anisotropy cannot be determined with a single profile and remains speculative. The possible anisotropy could be a result of LPO orientation of olivine crystals, which evolved during the formation of the oceanic crust. Alternatively, LPO orientation along our profile could somehow be related to the processes causing the large negative Geoid anomaly.

Data availability

Seismic and gravity datasets will be available via the PANGEA web portal.

CRediT authorship contribution statement

Tabea Altenbernd-Lang: Methodology, Investigation, Formal analysis, Data curation, Writing – original draft, Visualization, Validation. **Wilfried Jokat:** Conceptualization, Writing – review & editing, Project administration, Funding acquisition, Supervision, Validation. **Wolfram Geissler:** Project administration, Investigation, Conceptualization, Writing – review & editing, Funding acquisition. **Christian Haberland:** Investigation, Funding acquisition, Writing – review & editing. **Nalin De Silva:** Investigation, Writing – review & editing.

Declaration of Competing Interest

The authors declare that they have no known competing financial interests or personal relationships that could have appeared to influence the work reported in this paper.

Acknowledgements

We thank captain, officers, and crew of the RV Sonne for their work and support during expedition SO258/2. We thank the GIPP of GFZ for providing the land stations (grant GIPP201712) and the Geomar and Depas-Pool for providing the OBSs. We thank the Geological Survey and Mines Bureau of Sri Lanka (GSMB) for help and support during the installation and maintenance of the onshore seismic network. We thank three anonymous reviewers for their helpful comments. Funding was provided by the German Bundesministerium für Bildung und Forschung (BMBF) for this project (03G0258A). We acknowledge support by the Open Access Publication Funds of Alfred-Wegener-Institut Helmholtz-Zentrum für Polar- und Meeresforschung. All figures presented in this study were generated with the software GMT (Wessel et al., 2013).

References

Abdelmalak, M.M., Andersen, T.B., Planke, S., Faleide, J.I., Corfu, F., Tegner, C., et al., 2015. The ocean-continent transition in the mid- Norwegian margin: Insight from seismic data and an onshore Caledonian field analogue. Geology 43 (11), 1011–1014. https://doi.org/10.1130/G37086.1.

Altenbernd, T., Jokat, W., Geissler, W., 2020. The bent prolongation of the 85°E Ridge south of 5°N – Fact or fiction? Tectonophysics 785, 228457. https://doi.org/10.1016/j.tecto.2020.228457.

Banerjee, B., Sengupta, B.J., Banerjee, P.K., 1995. Signals of Barremian (116 Ma) or younger oceanic crust beneath the Bay of Bengal along 14 °N latitude between 81 °E and 93 °E. Mar. Geol. 128, 17–23. https://doi.org/10.1016/0025-3227(95)00086-E.

Berndt, C., Mjelde, R., Planke, S., Shimamura, H., Faleide, J.I., 2001. Controls on the tectono- magmatic evolution of a volcanic transform margin: the Vøring Transform margin. Geophys. Res. 22, 133–152.

Bull, J.M., Scrutton, R.A., 1990. Sediment velocities and deep structure from wide-angle reflection data around leg 116 Sites. Proc. Ocean Drill. Program Sci. Results 116, 311–316. https://doi.org/10.2973/odp.proc.sr.116.155.1990.

Chian, D., Louden, K.E., Minshull, T.A., Whitmarsh, R.B., 1999. Deep structure of the ocean-continent transition in the southern Iberia Abyssal Plain from seismic refraction profiles: Ocean Drilling Program (Legs 149 and 173) transect. J. Geophys. Res. Solid Earth 104, 7443–7462. https://doi.org/10.1029/1999JB900004.

Christensen, N.I., 1966. Elasticity of ultrabasic rocks. J. Geophys. Res. 71, 5921–5931. https://doi.org/10.1029/JZ071i024p05921.

Christensen, N.I., Mooney, W.D., 1995. Seismic velocity structure and composition of the continental crust: a global view. J. Geophys. Res. Solid Earth 100, 9761–9788. https://doi.org/10.1029/95JB00259.

Christeson, G.L., Goff, J.A., Reece, R.S., 2019. Synthesis of oceanic crustal structure from two-dimensional seismic profiles. Rev. Geophys. 57, 504–529. https://doi.org/10.1029/2019RG000641.

Contreras-Reyes, E., Grevemeyer, I., Watts, A.B., Planert, L., Flueh, E.R., Peirce, C., 2010. Crustal intrusion beneath the Louisville hotspot track. Earth Planet. Sci. Lett. 289, 323–333. https://doi.org/10.1016/j.epsl.2009.11.020.

Crosby, A., White, N., Edwards, G., Shillington, D.J., 2008. Evolution of the Newfoundland-Iberia conjugate rifted margins. Earth Planet. Sci. Lett. 273, 214–226. https://doi.org/10.1016/j.epsl.2008.06.039.

Curray, J.R., Emmel, F.J., Moore, D.G., Raitt, R.W., 1982. Structure, tectonics and geological history of the northeastern Indian Ocean, in. In: Nairn, A.E.M., Stehli, F.G. (Eds.), The Ocean Basins and Margins 6, the Indian Ocean. Plenum Press, New York, pp. 399–450.

Dean, S.M., Minshull, T.A., Whitmarsh, R.B., Louden, K.E., 2000. Deep structure of the ocean-continent transition in the southern Iberia Abyssal Plain from seismic refraction profiles: the IAM-9 transect at 40°20′N. J. Geophys. Res. Solid Earth 105, 5859–5885. https://doi.org/10.1029/1999JB900301.

Delescluse, M., Chamot-Rooke, N., 2008. Serpentinization pulse in the actively deforming Central Indian Basin. Earth Planet. Sci. Lett. 276, 140–151. https://doi.org/10.1016/j.epsl.2008.09.017.

Desa, M., Ramana, M.V., Ramprasad, T., 2006. Seafloor spreading magnetic anomalies south off Sri Lanka. Mar. Geol. 229, 227–240. https://doi.org/10.1016/j.margeo.2006.03.006.

Dick, H.J.B., Lin, J., Schouten, H., 2003. An ultraslow-spreading class of ocean ridge. Nature 426, 405–412.

Døssing, A., Stemmerik, L., Dahl-Jensen, T., Schlindwein, V., 2010. Segmentation of the eastern North Greenland oblique-shear margin – regional plate tectonic implications. Earth Planet. Sci. Lett. 292, 239–253.

Dreiling, J., Tilmann, F., Yuan, X., Haberland, C., Seneviratne, S.W.M., 2020. Crustal Structure of Sri Lanka Derived from Joint Inversion of Surface Wave Dispersion and Receiver Functions using a Bayesian Approach. J. Geophys. Res. Solid Earth 125. https://doi.org/10.1029/2019jb018688.

Eagles, G., Pérez-Díaz, L., Scarselli, N., 2015. Getting over continent ocean boundaries. Earth-Sci.Rev. 151, 244–265. https://doi.org/10.1016/j.earscirev.2015.10.009.

Eldholm, O., Thiede, J., Taylor, E., 1987. Evolution of the Norwegian continental margin: background and objectives. Proc., Initial Rep. (part A), ODP, Leg 104, Nor. Sea 5–25. https://doi.org/10.2973/odp.proc.ir.104.101.1987.

Fromm, T., 2016. PRay — a graphical user interface for interactive visualization and modification of rayinvr models. J. Appl. Geophys. 124, 1–3. https://doi.org/10.1016/j.jappgeo.2015.11.004.

Funck, T., Gohl, K., Damm, V., Heyde, I., 2012. Tectonic evolution of southern Baffin Bay and Davis Strait: results from a seismic refraction transect between Canada and Greenland. J. Geophys. Res. Solid Earth 117, 1–24. https://doi.org/10.1029/2011JB009110.

Gaherty, J.B., Lizarralde, D., Collins, J.A., Hirth, G., Kim, S., 2004. Mantle deformation during slow seafloor spreading constrained by observations of seismic anisotropy in the western. Atlantic 228, 255–265. https://doi.org/10.1016/j.epsl.2004.10.026.

Gaina, C., Müller, R.D., Brown, B., Ishihara, T., Ivanov, S., 2007. Breakup and early seafloor spreading between India and Antarctica. Geophys. J. Int. 170, 151–169. https://doi.org/10.1111/j.1365-246X.2007.03450.x.

Geissler, W., 2017. The Expedition SO258/2 of the Research Vessel SONNE to the Central Indian Ocean in 2017. Berichte zur Polar- und Meeresforschung. https://doi.org/10.2312/BzPM_0714_2017.

Geoffroy, L., 2005. Volcanic passive margins. Compt. Rendus Geosci. 337, 1395–1408. https://doi.org/10.1016/j.crte.2005.10.006.

Ghosh, A., Thyagarajulu, G., Steinberger, B., 2017. The Importance of Upper Mantle Heterogeneity in Generating the Indian Ocean Geoid Low. Geophys. Res. Lett. 44, 9707–9715. https://doi.org/10.1002/2017GL075392.

Gladczenko, T.P., Skogseid, J., Eldhom, O., 1998. Namibia volcanic margin. Mar. Geophys. Res. 20, 313–341. https://doi.org/10.1023/A:1004746101320.

Grevemeyer, I., Flueh, E.R., Reichert, C., Bialas, J., Kläschen, D., Kopp, C., 2001. Crustal architecture and deep structure of the Ninetyeast Ridge hotspot trail from active-source ocean bottom seismology. Geophys. J. Int. 144, 414–431. https://doi.org/10.1046/j.0956-540X.2000.01334.x.

Heintz, M., Kumar, V.P., Gaur, V.K., Priestley, K., Rai, S.S., Prakasam, K.S., 2009. Anisotropy of the Indian continental lithospheric mantle. Geophys. J. Int. 179, 1341–1360. https://doi.org/10.1111/j.1365-246X.2009.04395.x.

Hess, H.H., 1964. Seismic Anisotropy of the Uppermost Mantle under Oceans. Nature 629–631.

Hinz, K., 1981. A hypothesis on terrestrial catastrophes. In: Geologisches Jahrbuch Reihe E, Band E22, ISBN 978-3-510-96063-7.

Holbrook, W.S., Larsen, H., Korenaga, J., Dahl-Jensen, T., Reid, I.D., Kelemen, P., et al., 2001. Mantle thermal structure and active upwelling during continental breakup in

the North Atlantic. Earth Planet. Sci. Lett. 190 (3–4), 251–266. https://doi.org/10.1016/S0012-821X(01)00392-2.
Horen, H., Zamora, M., Dubuisson, G., 1996. Seismic waves velocities and anisotropy in serpentinized peridotites from Xigaze ophiolite: Abundance of serpentine in slow spreading ridge. Geophys. Res. Lett. 23, 9–12. https://doi.org/10.1029/95GL03594.
Ihnen, S.M., Whitcomb, J.H., 1983. Of the bathymetric profile is the exceptional depth of sedi- form and amplitude of the depression is varied. The disc. Geophys. Res. Lett. 10, 421–423.
Johnson, B.D., Powell, C.M.A., Veevers, J.J., 1980. Early spreading history of the Indian Ocean between India and Australia. Earth Planet. Sci. Lett. 47, 131–143. https://doi.org/10.1016/0012-821X(80)90112-0.
Jokat, W., Altenbernd, T., Eagles, G., Geissler, W., 2021. The early drift of the Indian Plate. Sci. Rep. 11, 10796. https://doi.org/10.1038/s41598-021-90172-z.
Jung, H., Karato, S.I., 2001. Water-induced fabric transitions in olivine. Science 293 (5534), 1460–1463. https://doi.org/10.1126/science.1062235.
Kelemen, P.B., Holbrook, W.S., 1995. Origin of thick, high-velocity igneous crust along the U.S. East Coast margin. J. Geophys. Res. 100, 10077–10094.
Klingelhoefer, F., Labails, C., Cosquer, E., Rouzo, S., Géli, L., Aslanian, D., Olivet, J.L., Sahabi, M., Nouzé, H., Unternehr, P., 2009. Crustal structure of the SW-Moroccan margin from wide-angle and reflection seismic data (the DAKHLA experiment) part a: Wide-angle seismic models. Tectonophysics 468, 63–82. https://doi.org/10.1016/j.tecto.2008.07.022.
Kopp, C., Fruehn, J., Flueh, E.R., Reichert, C., Kukowski, N., Bialas, J., Klaeschen, D., 2000. Structure of the makran subduction zone from wide-angle and reflection seismic data. Tectonophysics 329, 171–191. https://doi.org/10.1016/S0040-1951(00)00195-5.
Lau, K.W.H., Louden, K.E., Funck, T., Tucholke, B.E., Holbrook, W.S., Hopper, J.R., Christian Larsen, H., 2006. Crustal structure across the Grand Banks-Newfoundland Basin Continental Margin - I. results from a seismic refraction profile. Geophys. J. Int. 167, 127–156. https://doi.org/10.1111/j.1365-246X.2006.02988.x.
Leinweber, V.T., Jokat, W., 2012. The Jurassic history of the Africa-Antarctica corridor - new constraints from magnetic data on the conjugate continental margins. Tectonophysics 530–531, 87–101. https://doi.org/10.1016/j.tecto.2011.11.008.
Libak, A., Eide, C.H., Mjelde, R., Keers, H., Flüh, E.R., 2012. From pull-apart basins to ultraslow spreading: results from the western Barents Sea Margin. Tectonophysics 514–517, 44–61. https://doi.org/10.1016/j.tecto.2011.09.020.
Louden, K.E., 1995. Variations in crustal structure related to intraplate deformation: evidence from seismic refraction and gravity profiles in the Central Indian Basin. Geophys. J. Int. 120, 375–392. https://doi.org/10.1111/j.1365-246X.1995.tb01826.x.
Ludwig, J., Nafe, J., Drake, C., 1970. Seismic refraction. In: Maxwell, A.E. (Ed.), The Sea. Wiley-Interscience, New York, pp. 53–84.
Matthews, K.J., Seton, M., Müller, R.D., 2012. A global-scale plate reorganization event at 105-100 Ma. Earth Planet. Sci. Lett. 355–356, 283–298. https://doi.org/10.1016/j.epsl.2012.08.023.
McKenzie, D., 1979. Finite deformation during fluid flow. Geophys. J. R. Astron. Soc. 58, 689–715. https://doi.org/10.1111/j.1365-246X.1979.tb04803.x.
McKenzie, D., Sclater, J.G., 1971. The Evolution of the Indian Ocean since the late cretaceous. Geophys. J. R. Astron. Soc. 24, 437–528. https://doi.org/10.1111/j.1365-246X.1971.tb02190.x.
Mercier de Lépinay, M., Loncke, L., Basile, C., Roest, W.R., Patriat, M., Maillard, A., De Clarens, P., 2016. Transform continental margins – Part 2: a worldwide review. Tectonophysics 693, 96–115. https://doi.org/10.1016/j.tecto.2016.05.038.
Mishra, D.C., 2014. Geoid low and highs of the Indian Ocean and Western Pacific: Implications to mantle convection. J. Asian Earth Sci. 79, 441–445. https://doi.org/10.1016/j.jseaes.2013.10.020.
Mjelde, R., Raum, T., Myhren, B., Shimamura, H., Murai, Y., Takanami, T., Karpuz, R., Næss, U., 2005. Continent-ocean transition on the Vøring Plateau, NE Atlantic, derived from densely sampled ocean bottom seismometer data. J. Geophys. Res. Solid Earth 110, 1–19. https://doi.org/10.1007/BF02864837.
Mjelde, R., Raum, T., Murai, Y., Takanami, T., 2007. Continent-ocean-transitions: Review, and a new tectono-magmatic model of the Vøring Plateau, NE Atlantic. J. Geodyn. 43, 374–392. https://doi.org/10.1016/j.jog.2006.09.013.
Mueller, C.O., Jokat, W., 2019. The initial Gondwana break-up: a synthesis based on new potential field data of the Africa-Antarctica Corridor. Tectonophysics 750, 301–328. https://doi.org/10.1016/j.tecto.2018.11.008.
Mueller, C.O., Jokat, W., Schreckenberger, B., 2016. The crustal structure of Beira High, Central Mozambique—combined investigation of wide-angle seismic and potential field data. Tectonophysics 683, 233–254. https://doi.org/10.1016/j.tecto.2016.06.028.
Müller, R.D., Gaina, C., Tikku, A., Mihut, D., Cande, S.C., Stock, J.M., 2000. Mesozoic/cenozoic tectonic events around Australia. Geophys. Monogr. Ser. 121, 161–188. https://doi.org/10.1029/GM121p0161.
Mutter, J.C., Talwani, M., Stoffa, P.L., 1984. Evidence for a thick oceanic crust adjacent to the Norwegian margin. J. Geophys. Res. 89, 483–502. https://doi.org/10.1029/JB089iB01p00483.
Negi, J.G., Thakur, N.K., Agrawal, P.K., 1987. Can depression of the core-mantle interface cause coincident Magsat and geoidal "lows" of the Central Indian Ocean? Phys. Earth Planet. Inter. 45, 68–74. https://doi.org/10.1016/0031-9201(87)90198-1.
Norton, I.O., Sclater, J.G., 1979. A model for the evolution of the Indian Ocean and the breakup of Gondwanaland. J. Geophys. Res. Solid Earth 84, 6803–6830. https://doi.org/10.1029/JB084iB12p06803.
Oikawa, M., Kaneda, K., Nishizawa, A., 2010. Seismic structures of the 154–160 Ma oceanic crust and uppermost mantle in the Northwest Pacific Basin. Earth, Planets Sp. 62, e13–e16. https://doi.org/10.5047/eps.2010.02.011.
Pathak, A., Ravi Kumar, M., Sarkar, D., 2006. Seismic structure of Sri Lanka using receiver function analysis: a comparison with other high-grade Gondwana terrains. Gondwana Res. 10, 198–202. https://doi.org/10.1016/j.gr.2005.10.006.
Pavlenkova, N.I., 1996. General features of the uppermost mantle stratification from long-range seismic profiles. Tectonophysics 264, 261–278. https://doi.org/10.1016/S0040-1951(96)00131-X.
Pavlis, N.K., Holmes, S.A., Kenyon, S.C., Factor, J.K., 2012. The development and evaluation of the Earth Gravitational Model 2008 (EGM2008). J. Geophys. Res. Solid Earth 117, 1–38. https://doi.org/10.1029/2011JB008916.
Peirce, J.W., 1978. The northward motion of India since the Late Cretaceous. Geophys. J. R. Astron. Soc. 52, 277–311.
Peron-Pinvidic, G., Gernigon, L., Gaina, C., Ball, P., 2012. Insights from the Jan Mayen system in the Norwegian-Greenland Sea-I. Mapping of a microcontinent. Geophys. J. Int. 191, 385–412. https://doi.org/10.1111/j.1365-246X.2012.05639.x.
Peron-Pinvidic, G., Manatschal, G., Osmundsen, P.T., 2013. Structural comparison of archetypal Atlantic rifted margins: a review of observations and concepts. Mar. Pet. Geol. 43, 21–47. https://doi.org/10.1016/j.marpetgeo.2013.02.002.
Powell, C.M.A., Roots, S.R., Veevers, J.J., 1988. Pre-breakup continental extension in East Gondwanaland and the early opening of the eastern Indian Ocean. Tectonophysics 155, 261–283. https://doi.org/10.1016/0040-1951(88)90269-7.
Radhakrishna, M., Subrahmanyam, C., Damodharan, T., 2010. Thin oceanic crust below Bay of Bengal inferred from 3-D gravity interpretation. Tectonophysics 493, 93–105. https://doi.org/10.1016/j.tecto.2010.07.004.
Rai, A., Gaur, V.K., Rai, S.S., Priestley, K., 2009. Seismic signatures of the Pan-African orogeny: Implications for southern Indian high-grade terranes. Geophys. J. Int. 176, 518–528. https://doi.org/10.1111/j.1365-246X.2008.03965.x.
Raitt, R.W., Shor, G.G., Morris, G.B., Kirk, H.K., 1971. Mantle anisotropy in the Pacific Ocean. Tectonophysics 12, 173–186. https://doi.org/10.1016/0040-1951(71)90002-3.
Ramana, M.V., Nair, R.R., Sarma, K.V.L.N.S., Ramprasad, T., Krishna, K.S., Subrahmanyam, V., D'Cruz, M., Subrahmanyam, C., Paul, J., Subrahmanyam, A.S., Chandra Sekhar, D.V., 1994. Mesozoic anomalies in the Bay of Bengal. Earth Planet. Sci. Lett. 121, 469–475. https://doi.org/10.1016/0012-821X(94)90084-1.
Rao, G.S., Radhakrishna, M., Sreejith, K.M., Krishna, K.S., Bull, J.M., 2016. Lithosphere structure and upper mantle characteristics below the Bay of Bengal. Geophys. J. Int. 206, 675–695. https://doi.org/10.1093/gji/ggw162.
Rao, B.P., Kumar, M.R., Saikia, D., 2020. Seismic evidence for a hot mantle transition zone beneath the Indian Ocean Geoid Low. Geochem. Geophys. Geosyst. 21, 1–14. https://doi.org/10.1029/2020GC009079.
Reiss, A.S., Thomas, C., van Driel, J., Heyn, B., 2017. A hot midmantle anomaly in the area of the Indian Ocean Geoid Low. Geophys. Res. Lett. 44, 6702–6711. https://doi.org/10.1002/2017GL073440.
Reston, T.J., 2009. The structure, evolution and symmetry of the magma-poor rifted margins of the North and Central Atlantic: a synthesis. Tectonophysics 468, 6–27. https://doi.org/10.1016/j.tecto.2008.09.002.
Royer, J., Coffin, M., 1992. Jurassic to eocene plate tectonic reconstructions in the Kerguelen Plateau Region 1. Proc. Ocean Drill. Program 120, 917–923.
Sage, F., Basile, C., Mascle, J., Pontoise, B., Whitmarsh, R.B., 2000. Crustal structure of the continent-ocean transition off the Cote d'Ivoire-Ghana transform margin: Implications for thermal exchanges across the palaeotransform boundary. Geophys. J. Int. 143, 662–678. https://doi.org/10.1046/j.1365-246X.2000.00276.x.
Sandwell, D.T., Smith, W.H.F., 2009. Global marine gravity from retracked Geosat and ERS-1 altimetry: Ridge segmentation versus spreading rate. J. Geophys. Res. Solid Earth 114, 1–18. https://doi.org/10.1029/2008JB006008.
Shearer, P., Orcutt, J., 1985. Anisotropy in the oceanic lithosphere — theory and observations from the Ngendei seismic refraction experiment in the south-West Pacific. Geophys. J. R. Astron. Soc. 80, 493–526. https://doi.org/10.1111/j.1365-246X.1985.tb05105.x.
Shinohara, M., Fukano, T., Kanazawa, T., Araki, E., Suyehiro, K., Mochizuki, M., Nakahigashi, K., Yamada, T., Mochizuki, K., 2008. Upper mantle and crustal seismic structure beneath the Northwestern Pacific Basin using a seafloor borehole broadband seismometer and ocean bottom seismometers. Phys. Earth Planet. Inter. 170, 95–106. https://doi.org/10.1016/j.pepi.2008.07.039.
Simpson, E.S.W., Sclater, J.G., Parsons, B., Norton, I., Meinke, L., 1979. Mesozoic magnetic lineations in the Mozambique Basin. Earth Planet. Sci. Lett. 43, 260–264. https://doi.org/10.1016/0012-821X(79)90209-7.
Stern, T., Lamb, S., Moore, J.D.P., Moore, J.D.P., Okaya, D., Hochmuth, K., 2020. High mantle seismic P-wave speeds as a signature for gravitational spreading of superplumes. Sci. Adv. 6, 1–10. https://doi.org/10.1126/sciadv.aba7118.
Suckro, S.K., Gohl, K., Funck, T., Heyde, I., Ehrhardt, A., Schreckenberger, B., Gerlings, J., Damm, V., Jokat, W., 2012. The crustal structure of southern Baffin Bay: Implications from a seismic refraction experiment. Geophys. J. Int. 190, 37–58. https://doi.org/10.1111/j.1365-246X.2012.05477.x.
Tanimoto, T., Anderson, D.L., 1984. Mapping Convection in the Mantle. Geophys. Res. Lett. 11, 287–290.
Voss, M., Jokat, W., 2007. Continent-ocean transition and voluminous magmatic underplating derived from P-wave velocity modelling of the East Greenland continental margin. Geophys. J. Int. 170 (2), 580–604. https://doi.org/10.1111/j.1365-246X.2007.03438.x.
Wessel, P., Smith, W.H.F., Scharroo, R., Luis, J.F., Wobbe, F., 2013. Generic mapping tools : improved version released. EOS Trans. AGU 94, 409–410. https://doi.org/10.1002/2013EO450001.
White, R.S., Spence, G.D., Fowler, S.R., McKenzie, D.P., Westbrook, G.K., Bowen, A.N., 1987. Magmatism at rifted continental margins. Nature 330, 439–444.

White, R.S., McKenzie, D., O'Nions, R.K., 1992. Oceanic crustal thickness from seismic measurements and rare earth element inversions. J. Geophys. Res. 97, 19683. https://doi.org/10.1029/92JB01749.

Whitmarsh, R.B., Miles, P.R., 1995. Models of the development of the West Iberia rifted continental margin at 40°30′N deduced from surface and deep-tow magnetic anomalies. J. Geophys. Res. 100, 3789–3806. https://doi.org/10.1029/94JB02877.

Whitmarsh, R.B., Manatschal, G., Minshull, T.A., 2001. Evolution of magma-poor continental margins from rifting to seafloor spreading. Nature 413, 150–154. https://doi.org/10.1038/35093085.

Yelisetti, S., Spence, G.D., Scherwath, M., Riedel, M., Klaeschen, D., 2017. Dual-vergence structure from multiple migration of widely spaced OBSs. Tectonophysics 718, 45–60. https://doi.org/10.1016/j.tecto.2017.04.005.

Zelt, C.A., Smith, R.B., 1992. Seismic traveltime inversion for 2-D crustal velocity structure. Geophys. J. Int. 108, 16–34. https://doi.org/10.1111/j.1365-246X.1992.tb00836.x.